Si–C interactions during degradation of the diatom Skeletonema marinoi

Brivaëla Moriceau, Madeleine Goutx, Catherine Guigue, Cindy Lee, Robert Armstrong, Marie Duflos, Christian Tamburini, Bruno Charrière, Olivier Ragueneau

Si-C interactions during degradation of the diatom *Skeletonema marinoi*

Brivaëla Moriceau[1], Madeleine Goutx[2], Catherine Guigue[2], Cindy Lee[1], Robert Armstrong[1], Marie Duflos[2], Christian Tamburini[2], Bruno Charrière[2], and Olivier Ragueneau[3]

1- Marine Sciences Research Center, Stony Brook University, Stony Brook, NY 11794-5000, USA
2- Laboratoire Microbiologie, Géochimie et Ecologie Marines, UMR 6117 CNRS – INSU, Université de la Méditerranée, Centre d'Océanologie de Marseille, Campus de Luminy, 13288 Marseille, Cedex 9, France
3- Laboratoire des Sciences de l'Environnement Marin, UMR 6539, Institut Universitaire Européen de la Mer, Site du Technopole Brest-Iroise, Place Nicolas Copernic, 29280 Plouzané, France

Running title: Si-C interactions during diatom degradation

Deep Sea Research II special volume

For correspondence:

Brivaëla MORICEAU
LEMAR, UMR6539
Institut Universitaire Européen de la Mer (IUEM)
Technopole Brest Iroise
6 place Nicolas Copernic

Tel: (00 33) (0) 298 498 775
E-mail: moriceau@univ-brest.fr

Abstract

While a relationship between ballast and carbon in sedimenting particles has been well-documented, the mechanistic basis of this interaction is still under debate. One hypothesis is that mineral ballast protects sinking organic matter from degradation. To test this idea, we undertook a laboratory experiment using the diatom *Skeletonema marinoi* to study in parallel the dissolution of one of the most common mineral ballasts, biogenic silica ($bSiO_2$), and the associated degradation of organic matter. Three different models were applied to our results to help elucidate the mechanisms driving $bSiO_2$ dissolution and organic compound degradation. Results of this modelling exercise suggest that the diatom frustule is made up of two $bSiO_2$ phases that dissolve simultaneously, but at different rates. In our experiments, the first phase was more soluble ($k_{bSiO2} = 0.27\,d^{-1}$) and made up 31% of the total $bSiO_2$. In this phase, $bSiO_2$ was mainly associated with membrane lipids and the amino acids glutamic acid, tyrosine, and leucine. The second phase was more refractory ($k_{bSiO2} = 0.016\,d^{-1}$), and contained more neutral lipid alcohols and glycine. Until it dissolved, the first $bSiO_2$ phase effectively protected much of the organic matter from degradation: POC degradation rate constants increased from $0.025\,d^{-1}$ to $0.082\,d^{-1}$ after the total dissolution of this phase, and PON degradation rate constants increased from $0.030\,d^{-1}$ to $0.094\,d^{-1}$. Similar to POC and PON, the THAA degradation rate constant increased from $0.054\,d^{-1}$ to $0.139\,d^{-1}$ after dissolution of the first $bSiO_2$ phase. The higher THAA degradation rate constant is attributed to a pool of amino acids that was produced during silicification and enclosed between the two silica phases. This pool of amino acids might come from the incorporation of silica deposition vesicles into the diatom wall and might not be directly associated with $bSiO_2$. In contrast, most lipid degradation was not prevented by association with the more soluble $bSiO_2$ phase as the average lipid degradation rate constant decreased from $0.048\,d^{-1}$ to $0.010\,d^{-1}$ after 17 days of degradation; This suggests that most lipids were associated to rather than protected by silica, except pigments that appeared resistant

52 to degradation, independantly from silica dissolution. When the only organic compounds
53 remaining were associated with the second $bSiO_2$ phase, degradation rate constants decreased
54 greatly; concentrations changed only slightly after day 25.
55

Key Words: Biogenic silica, dissolution, carbon, amino acids, lipids, degradation, diatom

1. Introduction

Organic carbon produced in the ocean's surface layer by phytoplankton is conveyed to depth by particle sedimentation, and fluxes of carbon and minerals ($CaCO_3$, SiO_2 and aluminosilicates) are highly correlated in the deep water column. Based on these observations, Armstrong *et al.* (2002) highlighted the importance of modeling both carbon and mineral fluxes at the same time. Mineral ballast ($CaCO_3$ of coccolithophorids; SiO_2 of diatoms; aluminosilicates in dust) provide excess density needed for organic matter to sink; $bSiO_2$ and carbonate sedimentation are also linked through the ability of phytoplankton to aggregate and through grazing by zooplankton. The combination of these processes strongly increases the sedimentation rate of phytoplankton (e.g., Gehlen *et al.*, 2006; Moriceau *et al.*, 2007).

The role of mineral ballast in carbon transport is more complex than a simple impact on excess density (Lee *et al.*, 2008), but we are far from fully understanding the processes involved. Lee *et al.* (2000) and Hedges *et al.* (2001) hypothesized that mineral ballast could protect organic carbon from degradation; their hypothesis is consistent with the observation of Ingalls *et al.* (2006) that organic matter was more degraded in areas where diatoms were not the dominant bloom species when compared to sites where diatoms were the main phytoplankton group. Engel *et al.* (2008) also showed that the presence of the calcite test in coccolithophorids lowers the POC degradation rate during the recycling of these cells. Continuously increasing pressure reduced rates of $bSiO_2$ dissolution of diatom detritus relative to rates measured under atmospheric pressure conditions (Tamburini *et al.* 2006). In parallel, naturally collected sinking particles, were also less degraded by prokaryotes when pressure was continuously increased to simulate descent from 200 to 1500 (Tamburini *et al.* 2008). Despite all these findings, few studies (e.g., Ingalls *et al.*, 2003; 2006) have investigated both organic matter degradation and biogenic mineral dissolution in natural settings. The work of Engel *et al.* (2008) investigated the

role of $CaCO_3$ in carbon degradation, while the present study aims to better understand the role of Si-C interactions during diatom degradation.

Diatoms are the dominant species in many ecosystems; they are responsible for up to 35% of the total primary production in oligotrophic oceans and up to 75% in coastal waters and the Southern Ocean (Nelson *et al.*, 1995; Tréguer *et al.*, 1995). Jin *et al.* (2006) estimated their global contribution to net primary production and to carbon export to be 15% and 40%, respectively. The high diatom contributions to primary production and carbon export, could potentially explain the empiric relation established by Ragueneau *et al.* (2002). This relation shows that Si/C ratios decrease with depth and follow the same pattern everywhere in the world ocean. Is there a link between $bSiO_2$ dissolution and POC degradation such as the one hypothesized in the work cited above?

The objective of the present study was to understand how biogenic silica influences the degradation of diatom organic carbon, and conversely the role of organic compounds in $bSiO_2$ dissolution. With this aim, a monospecific culture of the diatom *Skeletonema marinoi* was incubated in the presence of a natural coastal bacterial community and allowed to degrade over a 102-day period. $bSiO_2$ dissolution and the quantity and composition of organic compounds, including amino acids and lipids, were assessed throughout the incubation period and used to investigate Si-C interactions during decomposition. Three dissolution/degradation models were applied to the experimental data to elucidate the dissolution/degradation pattern of the components of *S. marinoi*. This modeling experiment yields a better understanding of the structure of the diatom frustule in *S. marinoi* and of the role of Si-C interactions during diatom recycling.

2. Material and methods

2.1 Biodegradation experiment

105 *Skeletonema marinoi* (CCAP 1077/3) obtained from IFREMER (Argenton station, France) was
106 grown in f/2 medium (Guillard and Ryther, 1962; Guillard, 1975) under 12/12 dark/light
107 illumination. When cells reached stationary growth phase (6.5×10^6 cells ml^{-1}), they were
108 transferred into a 4°C chamber and kept in the dark for 5 days. During this period, cells sank to
109 the bottom of the flask, and previous tests showed that diatom viability (number of living cells
110 versus total cells) decreased (unpublished data, method described in Garvey *et al.* 2007). The
111 supernatant was poured off, and the overlying medium was replaced with natural seawater that
112 had been passed through a 0.7-µm GFF filter to preserve the natural bacteria assemblage. The
113 seawater was collected from a small inlet (Endoume) near Marseille, France, at the end of fall,
114 when the water is naturally poor in silicic acid (dSi~2.5 µM). The mixture of *S. marinoi* and
115 filtered sea water was then transferred to an incubation flask equipped with a magnetic stirrer
116 and a stopper through which gas exchange could occur via a 0.2-µm Swinnex® filter. The
117 diatoms were incubated for 102 days in the dark at 20°C. Using a peristaltic pump, samples were
118 taken daily for the first 21 days and then at 23, 25, 46, 50, and 102 days; triplicate samples were
119 taken at 0, 5, 11, 46, 50, and 102 days. The sampled solution was well-mixed, allowing the ratio
120 of solid matter to solution to remain constant (Dixit *et al.*, 2001). Ten percent of the liquid
121 volume remained at the end of the experiment. Chemical parameters measured were biogenic
122 silica ($bSiO_2$), silicic acid (dSi), particulate organic carbon and nitrogen (POC, PON), dissolved
123 organic carbon (DOC), total particulate lipids (TLip), and total hydrolyzable amino acids
124 (THAA). In addition total bacterial abundances (diamidinophenylindole: DAPI counts) were
125 counted. Si contamination by dissolution of glassware was measured by analyzing dSi in an
126 incubation bottle with no cells added. We also sampled controls poisoned with 20 mg l^{-1} $HgCl_2$
127 at 4 times (0, 2, 5, and 11 days) to verify that degradation was due to bacteria and not abiotic
128 factors.
129
130 **2.2 Analytical Methods**

131 *Biogenic Silica ($bSiO_2$)* was determined at the beginning and end of the experiment using
132 a variation of the method of Ragueneau and Tréguer (1994). As no lithogenic silica was present
133 in the algal culture, the second digestion step using HF was not necessary. Ten-ml samples were
134 filtered onto 0.2-µm polycarbonate filters. Filters were analyzed for $bSiO_2$ and the filtrate for
135 dSi. For $bSiO_2$, filters were digested in 20 ml of 0.2N NaOH for three hours at 95°C to ensure
136 the dissolution of all $bSiO_2$; dSi concentrations in the solution remained far below the solubility
137 equilibrium of $bSiO_2$ at all times. After cooling, the solution was acidified with 5 ml of 1N HCl,
138 centrifuged to remove remaining solids, and analyzed for dSi. The precision for triplicate
139 measurements of $bSiO_2$ was < 5%.
140 *Silicic acid* (dSi*)* concentrations were determined on 10-ml filtered samples and on
141 digested $bSiO_2$ samples using the molybdate blue spectrophotometric method of Mullin and
142 Riley (1965), as adapted by Tréguer and Le Corre (1975) and modified by Gordon *et al.* (1993)
143 for use in segmented flow colorimetry. We used a Bran and Luebbe Technicon Autoanalyzer
144 (<1% precision).
145 *POC* and *PON* concentrations were measured using a Carlo Erba NA 2100 CN analyzer
146 coupled to a Finnigan Delta S mass spectrometer. Five-ml samples were filtered through 0.7-µm
147 GFF filters. The filters were desiccated overnight in an oven at 50°C and then placed in tin
148 capsules to be introduced into the oven of the analyzer. The precision for triplicate N analyses
149 was ± 1-6%, and for C analysis ± 1-5%.
150 *DOC* was analyzed after filtration through 0.7-µm GFF filters; 10 ml of each sample was
151 transferred into glass ampoules and sealed after addition of H_3PO_4 as preservative. All glassware
152 was pre-rinsed with 1N HCl and Milli-Q water before being combusted at 465°C; care was taken
153 to minimize contamination during sampling and handling. DOC was measured by high-
154 temperature catalytic oxidation using a Shimadzu TOC 5000 Analyzer (Sempéré *et al.*, 2003;
155 Sohrin and Sempéré, 2005). Samples were acidified to pH 1 with 85% phosphoric acid and
156 bubbled for 10 minutes with CO_2-free air to purge them of inorganic carbon. Three or four 100

157 µl replicates of each sample were injected into the 680 °C column. The precision of these
158 replicates was ≤ 6%.

159 *Total particulate lipids* were analyzed after filtering 10 ml samples onto 0.7-µm GFF
160 glass fiber filters. Filters were extracted according to Bligh and Dyer (1959). Lipid extracts
161 were separated into classes of compounds and quantified on an Iatroscan model MK-6s (Iatron,
162 Tokyo; H_2 flow 160 ml min^{-1}; air flow 2 l min^{-1}) as described by Goutx *et al.* (2007). The
163 elution scheme allows reliable separation and quantification of degradation metabolites from
164 acyl-lipid classes (Striby *et al.*, 1999). Total particulate lipids (TLip) are the sum of the
165 separated lipid classes (Table 1). In the present work, the variability within triplicates was <
166 13%.

167 *Amino acids* were analyzed on 0.7-µm GFF filters after filtration of 10-ml samples.
168 Thawed filters were treated as described in the study of Ingalls *et al.* (2003). Individual
169 compounds were separated by HPLC using pre-column OPA derivatization after acid hydrolysis
170 as described in Lee and Cronin (1982) and Lee *et al.* (2000). Amino acids were detected by
171 fluorescence and identified by comparison to retention times of standards made from an amino
172 acid mixture (Pierce, Standard H). The non-protein amino acids β-alanine and γ-aminobutyric
173 acid (BALA and GABA) were added individually to the standard mixture. Aspartic acid (ASP)
174 and glutamic acid (GLU) measurements include the hydrolysis products of asparagine and
175 glutamine. THAA is the sum of the 16 characterized amino acids (Table 1). Variation among
176 replicates was generally 15-30%. LYS replicates, however, varied more greatly at times, e.g.,
177 50% at day 11.

178 *Total bacterial abundances (DAPI counts):* Subsamples for bacterial cell counts were
179 fixed immediately with buffered formalin (final volume 2%). Cells were collected onto a 25-mm
180 0.2-µm polycarbonate Nuclepore® membrane and stained with diamidinophenylindole (DAPI;
181 Porter and Feig, 1980). Slides were stored frozen until counting by epifluorescence microscopy
182 (Olympus, BH2).

183

184 **2.3 Kinetics**

185 Kinetic parameters were calculated over the first 25 days where experimental data are
186 available every 1-2 days. For each compound of interest we tested three degradation/dissolution
187 models. Model 1 is a simple first-order rate equation as described in Greenwood *et al.* (2001)
188 and used in many dissolution studies (e.g. Kamatani and Riley, 1979; Kamatani *et al.*, 1980;
189 Kamatani, 1982):

190 $$\hat{C}(t) = C_0 \exp(-k\,t)\,, \qquad (1)$$

191 where $\hat{C}(t)$ is the concentration (μM) estimated at time t (d), C_0 is the initial concentration, and
192 k is the dissolution/degradation rate constant (d^{-1}).

193 Model 2 assumes simultaneous dissolution/degradation of two phases. The equation used
194 is similar to that used for carbon degradation in the study of Westrich and Berner (1984):

195 $$\hat{C}(t) = C_1 \exp(-k_1 t) + C_2 \exp(-k_2 t) \qquad (2)$$

196 In Model 2, four parameters are estimated: $C_1$and C_2 are concentrations (μM) of phase or pool 1
197 and 2, and k_1 and k_2 (d^{-1}) are their respective dissolution or degradation rate constants.

198 As it uses 2 more parameters, Model 2 always gives a better fit than Model 1 except
199 when the initial degradation rate is slower than later rates. In this specific case Model 2
200 performs no better than Model 1. We therefore developed Model 3, which employs one first-
201 order equation initially, and a second first-order equation after that. The time at which the
202 dissolution/degradation rate constant changes is called the substitution time (t_s), and is allowed
203 to take on any value >0.

204 $$\hat{C}(t) = C_0 \exp(-k_1 t), \quad 0 < t < t_s\,; \qquad (3a)$$

205 $$\hat{C}(t) = C(t_s) \exp(-k_2 t), \quad t > t_s\,. \qquad (3b)$$

206 Model 3 also contains 4 parameters.

If dissolution/degradation for a given compound is best reconstructed using Model 2, this compound is constituted by at least two phases or pools; on the other hand if Model 3 gives a better description of the dissolution/degradation pattern, either the compound studied is present in 2 phases/pools remineralizing one after the other, or a change in environmental parameters provoked a change in the dissolution/degradation rate constant at time *ts*.

In addition, to allow direct comparison of the degradation/dissolution pattern among all compounds, and between this study and previous studies, an initial disappearance rate constant was calculated for each compound over the first 10 days using Model 1.

2.4 Statistics

Each fit was optimized by maximizing the likelihood statistic log(L) as described in equation 4 (Armstrong *et al.*, 2002, and references therein). Eq. (4) is based on a Gaussian distribution with a constant variance on a logarithmic scale:

$$\log(L) = -\frac{N}{2} \times \log\left(\frac{\sum (\log(\hat{C}_j) - \log(C_j))^2}{N} \right) , \qquad (4)$$

where N is the number of data points, C_j is a measured concentration for data point j, and the $\hat{C}_j$ is the corresponding model prediction. The difference in log(L) ($\Delta \log(L)$) between fits of two different models to the same data gives the goodness of fit of one model compared to the other. If one model gives a value for log(L) that is at least 2 points higher per added parameter than another model, it is considered to fit the data better (Hilborn and Mangel, 1997). In the present work, the simplest model (Model 1) was considered to be the best fit unless Model 2 or Model 3 yielded a log(L) more than 4 points better than that of Model 1.

3. Results

230 **3.1 Change in biochemical composition of the diatom *Skeletonema marinoi* over time**

231 *3.1.1 General trends*

232 Changes in $bSiO_2$, POC, TLip and THAA concentrations over time are shown in
233 logarithmic scale in Fig. 1. While $bSiO_2$ concentrations decreased smoothly over the first 25 d,
234 POC, PON and THAA concentrations decreased until about day 14, when the loss rate increased,
235 especially for THAA. In contrast, TLip concentration decreased rapidly at the beginning of the
236 experiment and reached a plateau after day 13.

237 Bacterial concentrations started at $0.33 \pm 0.03 \times 10^6$ cell ml^{-1} and peaked at day 14 with
238 a concentration of $30 \pm 2.7 \times 10^6$ cell ml^{-1} (Fig. 2). The bacterial population increased between
239 days 0 and 14 with a rate equal to $0.015\ d^{-1}$ (calculated between days 2 and 14) and then
240 generally stabilized reaching a final concentration of $20 \pm 4 \times 10^6$ cell ml^{-1} until the end of the
241 experiment. The bacterial growth efficiency (bacterial carbon increase divided by POC decrease)
242 between days 0 and 14 was 2%. Bacterial carbon made up a maximum of 2.4 ± 0.6% of the POC.

243 TOC concentrations over time showed a pattern similar to those of POC (Fig. 3). DOC
244 concentrations increased slightly (5.6 ± 0.2 mg C L^{-1}) but much less than POC decreased (62 ± 3
245 mg C L^{-1}). The bacterial carbon (C_{bact}) is so low compared to the algal organic carbon that the
246 mineralization rate for POC algal (POC+DOC- C_{bact}) is the same as for the total organic carbon
247 (Corg = POC+DOC). This rate calculated as the slope of TOC change over time (Fig. 3) was
248 2.68 mg C $L^{-1}\ d^{-1}$ during the first 20 days of the experiment and was equivalent to 91% of the
249 POC loss.

250

251 *3.1.2 Initial biochemical composition*

252 At the beginning of the experiment, the Si/POC ratio was 0.09 ± 0.01, which is slightly
253 lower than the value of 0.13 measured in fresh diatoms by Brzezinski (1985) but in the range of
254 coastal diatoms measured by Rousseau *et al.* (2002). TLip made up 19 ± 2% of *S. marinoi*

organic carbon which is a little bit higher that Lip/POC ratios measured previously for the same specie (Lavens and Sorgeloos, 1996). TLip mainly included FFA and other degradation metabolites (ALC and MG; see Table 1 for abbreviations) (Fig. 4a). Cellular membrane phospholipids (PE, DPG+PG) and chloroplast membrane glycolipids (MGDG) accounted for 10 ± 1% and 13 ± 1% of TLip, respectively. FFA were the most abundant lipid degradation metabolites (24.8 ± 0.5%) among those present. PIG included both chlorophyll *a* and its degradation products (Striby *et al.*, 1999); PIG was the largest lipid class (initially 41 ± 5%; Fig. 4a). ST are involved in membrane rigidity (Parrish, 1988); they were initially minor components of *S. marinoi*.

THAA constituted a larger portion (36 ± 9%) of total organic carbon than the lipids, similar to the 45% found in *Thalassiosira weissflogii* by Cowie and Hedges (1996) and the 25% observed in diatom-rich sediments by Ingalls *et al.* (2006). THAA include the monomer constituents of protein as well as adsorbed amino acids and peptides. Sixteen amino acids were quantified. GLU, ASP and LEU (see Table 1 for abbreviations) together made up one third of the THAA, each more than 11 ± 3% (Table 2). Other amino acids were between 2.1 ± 0.6% and 9.3 ± 2.8% of the THAA except for MET and GABA, which were less than 0.8%. As GABA and MET concentrations were very low throughout the incubation, they are not described in the following paragraphs. The initial mole% amino acid compositions we found for *S. marinoi* (Table 2) were very similar in pattern to those of cultured diatoms reported by Ingalls *et al.* (2003) and Cowie and Hedges (1996), with highest mole% values for ASP, GLU, and GLY. *S. marinoi* was higher in mole% LEU than in reports of other diatoms. THAA do not include the amino acids incorporated inside the silica frustule, unless part of the frustule is dissolved during acid hydrolysis (see later discussion). We define Si-bound amino acids as Si-THAA as in Ingalls *et al.* (2003).

3.1.3 Change in biochemical composition during degradation

281 Si/POC decreased from 0.09 ± 0.01 mol of Si/mol of C to 0.06 ± 0.01 mol of Si/mol of C
282 during the first 2 days of incubation and then stabilized until day 15 of the experiment. After
283 increasing to 0.11 ± 0.01 mol of Si/mol of C between days 15 and 21, the Si/POC ratio remained
284 constant until the end of the experiment. TLip/POC varied between 0.13 ± 0.02 mol of C/mol of
285 C and 0.23 ± 0.03 mol of C/mol of C during the first 50 days. Then the ratio decreased to a final
286 value of 0.06 ± 0.01 mol of C/mol of C at day 102. THAA/POC decreased regularly during the
287 whole experiment from 0.36 ± 0.09 mol of C/mol of C initially to 0.10 ± 0.02 mol of C/mol of C
288 after 102 days, except for a sudden increase between day 11 and 15 from 0.28 ± 0.7 mol of
289 C/mol of C to 0.38 ± 0.10 mol of C/mol of C.
290 Most of the change in TLip composition (Fig. 4a) occurred between days 0 and 25. Most
291 compounds decreased or remained the same relative to TLip (mol of C/mol of C) except for PIG,
292 which increased from 41 ± 5% to 80 ± 7% of the TLip over the course of the experiment.
293 Relative concentrations (mol of C/mol of C) of FFA, the second most abundant lipid class in the
294 algae, decreased regularly from 24.8 ± 0.5% to 4.0 ± 0.4%. MGDG initially made up 13 ± 1% of
295 TLip, but totally disappeared by day 4. The MG contribution was constant (7.0 ± 0.3%) until day
296 14, when it was completely degraded. The contribution of membrane lipids, the glycolipid
297 MGDG and the phospholipids (PE and DPG+PG) to TLip was low compared to results from
298 Berge *et al.* (1995) and d'Ippolito *et al.* (2004). However, lipid composition is highly dependent
299 on culture conditions (d'Ippolito *et al.*, 2004), and in our case the high FFA content probably
300 masked the relative contribution from membrane lipids.
301 The THAA composition was relatively constant throughout the degradation experiment
302 except between days 15 and 20 where we observed a strong peak of GLY, which increased from
303 13 ± 2% to 33 ± 8% (Fig. 4b). The relative concentrations of HIS (data not shown) and LYS also
304 peaked slightly between days 15 and 20. Relative proportions of other amino acids especially
305 ASP decreased at this time in response to the increases in HIS, GLY and LYS.
306

307 **3.2 Dissolution and degradation kinetics of *S. marinoi* constituents**

308 *3.2.1 Silica kinetics*

309 The experiment was conducted in glass bottles to eliminate carbon contamination.
310 Controls showed that after 102 days, dSi due to leaching from the glass was a maximum of 5%
311 of the dSi due to dissolution of diatom frustules. From an initial concentration of 680 ± 30 µmol
312 L^{-1}, $bSiO_2$ decreased rapidly during the first 3 to 5 days of the experiment and then more slowly
313 (Fig. 1). After 25 days, 52% of the initial $bSiO_2$ was dissolved and 76% of the initial was
314 dissolved at the end of the experiment (102 d). The comparison between the $\log(L)$ of the three
315 models describing $bSiO_2$ dissolution showed that Model 2 is 4.3×10^{16} times better than Model 1
316 ($\Delta\log(L) = 38.3$) and almost 4.5×10^{5} times better than Model 3 ($\Delta\log(L) = 13$). $bSiO_2$ was the
317 only constituent of the diatom with a dissolution pattern that was best described by Model 2
318 (Fig.5a, Table 4) meaning that the frustule is most likely composed of two phases dissolving
319 simultaneously. The first phase of $bSiO_2$ constituted 31% of the total $bSiO_2$ and was more
320 soluble, with a dissolution rate constant of $0.27\,d^{-1}$. The second phase was more refractory with
321 a dissolution rate constant of $0.016\,d^{-1}$ (Table 4). For direct comparison with POC and PON,
322 the initial loss rate constant of the total $bSiO_2$ was calculated using Model 1 over 10 days as
323 $0.049\,d^{-1}$. The three dissolution constants are within the range ($0.005\,d^{-1}$ to $1.3\,d^{-1}$) given in
324 the review by Van Cappellen *et al.* (2002b).
325
326 *3.2.2 POC and PON kinetics*

327 POC concentration decreased in two steps from the initial value of 7660 ± 150 µmol L^{-1}
328 (Fig. 1). Even with more parameters Model 2 did not improve the fit to the data obtained by
329 Model 1 (Fig. 5b); $\log(L)$ calculations for POC loss showed that Model 3 gave the best fit
330 ($\Delta\log(L) = 76.5$). This suggests that either two pools of POC exist and are degraded
331 successively, or a change in some parameter not directly linked to POC chemistry provoked an

332 increase of the degradation rate at day 10 from 0.025 to 0.082 d^{-1} (Table 4). PON followed the
333 same pattern; Model 3 reproduced the data with more accuracy as shown by the $\Delta\log(L)$ of 37.3
334 compare to Models 1 and 2. Model 3 estimated an increase in PON degradation rate at day 12
335 from 0.03 to 0.094 d^{-1} (Table 4). The first POC degradation rate constants are similar to rate
336 constants measured in previous studies (0.036 d^{-1} for POC, Lee and Fisher, 1992; 0.035 d^{-1} for
337 POC and 0.047 d^{-1} for PON, Harvey *et al.*, 1995). For comparison with $bSiO_2$, we also applied
338 Model 1 over 10 days to calculate the initial loss rate of POC and PON: 0.025 d^{-1} for POC and
339 0.029 d^{-1} for PON.
340 The POC degradation pattern in the Hg-poisoned controls was similar to that in
341 unpoisoned flasks during the first 5 days but was lower between days 5 and 11. The degradation
342 rate constant measured over the first 11 days using Model 1 was 0.021 d^{-1}.
343
344 *3.2.3 Lipid kinetics*
345 From an initial TLip concentration of 1400 ± 70 μmol C L^{-1}, almost half (42 ± 4%)
346 degraded in 25 days; 7.0 ± 0.3 % of TLip remained after 102 days. The degradation of 7 of the 8
347 lipid classes is shown in Fig. 6a. TLip degradation is better described by Model 2 and 3 than by
348 Model 1 ($\Delta\log(L)$ = 15.6 and 17 respectively). With only 1.5 point of $\log(L)$ difference between
349 Model 2 and 3 but the same degree of complexity (4 parameters each) we chose the best fit from
350 the best likelihood which was given by Model 3 (Table 4). The degradation rate constant for
351 TLip was 0.048 d^{-1} during the first 17 days of the experiment and then decreased to 0.01 d^{-1}.
352 The initial degradation rate constant was 0.046 d^{-1}, slightly higher than the 0.023 d^{-1} measured
353 in the study of Harvey *et al.* (1995).

354 Using Model 1 we calculated that FFA, PIG, MG and PG+DPG had degradation rate
355 constants of 0.104, 0.012, 0.045 and 0.011 d^{-1} over 25 days respectively. For MGDG, ST, PE,
356 and ALC, Model 3 gives the best fit to the data (Table 4).
357 MGDG turned over slowly (0.078 d^{-1}) during the first 2 days, but then much more
358 quickly (0.52 d^{-1}; Table 4) and were completely gone after only 4 days. MG were also
359 completely lost very quickly; the initial degradation rate constant of MG was 0.045 d^{-1}, but the
360 remaining MG was gone after 14 days. This pattern does not fit any of the models used, and
361 suggests an association of these lipids only with the first $bSiO_2$ phase, or no association at all.
362 MGDG, ST, and PE degradation rate constants increased by a factor of 8 to 10 during the
363 experiment. They followed the same pattern as POC and PON. ALC degradation rate constant
364 decreased after 19 days.
365 *3.2.4 Amino acid kinetics*
366 From the initial THAA concentration of 3020 ± 200 μmol C L^{-1}, 86 ± 17 % of the THAA
367 were degraded after 25 days; 5.0 ± 0.5 % of the THAA still remained after 102 d. As for POC
368 and PON, Model 3 was the best fit for THAA degradation ($\Delta\log(L) = 9.9$ with both Model 1 and
369 Model 2). Concentrations of THAA decreased from day 1 to day 13 with an average degradation
370 rate constant of 0.054 d^{-1}. After 13 d THAA turned over with a faster degradation rate constant
371 of 0.139 d^{-1} (Table 4), before reaching a period of very low rate constants after day 25; THAA
372 concentrations were almost constant until day 102. This last rate was not calculated by models
373 as the modelling exercise was applied only over the first 25 days. The first degradation phase of
374 THAA was similar to that measured on *T. weissflogii* (0.058 d^{-1}) by Harvey *et al.* (1995).
375 Initially, the degradation rate constant of the 14 individual amino acids ranged between 0.015
376 and 0.070 d^{-1}, except for ASP and SER, which turned over more slowly with constants of 0.001
377 and 0.007 d^{-1}, respectively (Table 4). At day 11 when on average 49 ± 10 % of the THAA had

degraded, all concentrations except ARG and SER suddenly increased by 6 to 58 % in 1 to 2 days (Fig. 6b). The largest releases were observed for HIS, GLY and LYS, which increased by 39 ± 13 %, 58 ± 10 % and 46 ± 12 %, respectively. For every amino acid except TYR, degradation rate constants increased after this peak. For ASP and SER the increase occurred earlier at day 5, and for TYR the degradation rate constant decreased from 0.070 to $0.012\,d^{-1}$ at day 21. Except for TYR, amino acids turned over faster during the second degradation phase, and degradation rate constants ranged between 0.110 and $0.182\,d^{-1}$. The degradation rate constant of SER increased even more than the other amino acids reaching $0.897\,d^{-1}$ (Table 4).

3.3 Relation between $bSiO_2$ dissolution and degradation of individual organic compounds or compound classes

3.3.1 Lipid degradation versus $bSiO_2$ dissolution

There was a strong linear relationship between total $bSiO_2$ and TLip over the whole range of $bSiO_2$ concentrations (r^2 = 0.85, n = 26) measured. There was no correlation between $bSiO_2$ and PIG, so that the relationship between $bSiO_2$ and TLip became even better when pigments were excluded from the other lipids (r^2 = 0.94, n = 26). FFA were well correlated with total $bSiO_2$ concentrations (r^2 = 0.95, n = 26); they were completely degraded during the dissolution of the second $bSiO_2$ phase, when $bSiO_2$ concentrations eventually reached 260 μmol L^{-1}.

Relationships among individual lipid classes and $bSiO_2$ phases showed three distinct periods (Fig. 7a and b), which were related to $bSiO_2$ dissolution using the $bSiO_2$ model (Figure 5a). Period 1 (P1) is the time corresponding to dissolution of 85% of the first $bSiO_2$ phase and 10% of the second $bSiO_2$ phase; Period 2 (P2) is the time corresponding to dissolution of most of the remaining $bSiO_2$ from the first phase and another 10% of the second $bSiO_2$ phase; and Period 3 (P3) is the time when less than 1.5% of the first phase remained and 60% of the second phase dissolved. At the end of P3 20% of the $bSiO_2$ from the second phase remained. On average, 26-34% of the TLip degraded during Period 1; only 14-19% of TLip remained at the beginning of

403 Period 3. The slow decrease of concentrations observed for each lipid class except PIG, during
404 P1 and P3 compared to P2 despite the fact that the three periods lasted the same time (~7 days,
405 Fig. 5a), might show that most TLip except PIG degraded during P1 were associated with the
406 first $bSiO_2$ phase, and most TLip except PIG degraded during P3 with the second $bSiO_2$ phase.
407 These specific lipids are denoted as Si(1)-Lip and Si(2)-Lip; their composition is shown Table 3.
408 Of the individual classes, PE, ALC concentrations remained almost constant during P1.
409 In contrast, MGDG was completely degraded within the first 4 days, in P1. Despite the high
410 variability in PE and ST concentration measurements, we determined that ST and MG
411 concentrations decreased only slightly in P1 (>27%). This trend is illustrated by their low
412 degradation constants ($0.016\,d^{-1}$ and $0.001\,d^{-1}$, respectively).
413 Degradation of MG, ALC, PE and ST mainly occurred in P2. PE and ST concentrations
414 dropped in P2 and ALC degradation was even faster; Model 3 gave a higher k_1 and a longer *ts*
415 for ALC than for PE and ST. After the precipitous drop, which corresponded to the beginning of
416 P3, 80% of ALC, FFA and PE and 40% of ST were degraded. MG were completely degraded so
417 quickly at the beginning of P2 that the loss is more likely due to sudden release of MG adsorbed
418 onto particles or dissolution (i.e. involving chemical mechanisms) rather than degradation (i.e.
419 biological mechanisms).
420 DPG+PG were not well correlated with $bSiO_2$; generally there was a 36%-degradation
421 during P1, then a fast release of DPG+PG in P2 (40-50%), possibly when the first $bSiO_2$ phase is
422 completely dissolved. Due to the release in P2, 80% of the initial DPG+PG remained at the
423 beginning of P3.
424
425 *3.3.2 Amino acid degradation versus $bSiO_2$ dissolution*
426 The relationship of THAA with the two $bSiO_2$ phases showed changes at the same times
427 as many of the lipid classes, so we used the same three periods. During Period 1, when the first
428 $bSiO_2$ phase was dissolving, only 3-22 % of the THAA degraded. For the reason described in the

previous section for lipids (3.3.1), this portion of the THAA is referred to as Si(1)-THAA. GLY and LYS lost less than 10 % of their initial concentrations; ASP and GLU lost 40 % of their initial concentrations. GLU, ASP, and LEU constituted most of the pool degrading during P1; LYS is not correlated to the first $bSiO_2$ phase (Table 2).

At the end of period 2, a pool of THAA was released when 95 % of the first $bSiO_2$ phase was dissolved (Fig. 8a and b). THAA concentrations decreased by 32 % compared to initial values. Measurement of THAA does not release Si-bound amino acids so that they would not be observed until the $bSiO_2$ dissolved; the THAA released (Si(2)-THAA) may have been trapped between the 2 phases. The amount of Si(2)-THAA can be calculated from the difference between the concentrations of amino acids at and before the peak maximum (Table 2). In total, THAA concentration increased by 11-16 % (in $\mu mol\ C\ L^{-1}$); the Si(2)-THAA were composed mainly of GLY (23 ± 8 %) and LYS (23 ± 8 %; see Table 2).

During P3, relative THAA concentrations declined from 34 % to 5 % of the original THAA. The THAA lost during P3 are called Si(3)-THAA, they had a composition similar to that of total THAA, except that the contribution of GLY was higher (Table 2).

4. Discussion

4.1 Importance of bacteria in *S. marinoi* degradation

The very high concentration of algae, when compared to the bacterial concentrations, and the continued degradation in the presence of $HgCl_2$, suggest that the loss of organic matter was due not only to biological degradation, but also to physical and chemical factors (dissolution). In the presence of $HgCl_2$, organic matter turned over with a low rate constant ($0.02\,d^{-1}$, $r^2 = 0.86$, $n = 8$), which appeared to decrease even more after day 5 ($0.007\,d^{-1}$, $n = 4$; 2 replicates). This could be due to initial dissolution of organic matter as the cell begins to fall apart; smaller rate constants after some time would then be due to the absence of bacterial degradation. However,

454 the lack of appropriate samples makes this observation tentative. The slower increase of DOC
455 concentrations compared to the decrease in POC (Fig. 3) suggests that most of the POC loss may
456 be due to bacterial degradation despite the similar degradation rate measured in $HgCl_2$-poisoned
457 batches. Degradation of particulate matter in the presence of $HgCl_2$ has been noted before (Liu
458 *et al.*, 2006).

459 It was not clear why bacteria grew so slowly after day 14 in the unpoisoned experiment.
460 Three factors could have contributed to the decrease and stabilization of bacterial growth. First,
461 O_2 could have been a limiting factor. We did not measure O_2 during the experiment but we
462 calculated average TOC loss, R_{loss} = 221.6 μmol L^{-1}. Change in oxygen concentrations (C_{O2})
463 with time (t) can be reconstructed from O_2 consumption rate (R_{loss}) and O_2 diffusion rate (R_{diff})
464 (eq. 5). The latter is given by the Whitman film model (Gladyshev 2002; eq. 6).

465 $$\frac{dC_{O2}}{dt} = R_{diff} - R_{loss} \qquad (5)$$

466 $$R_{diff} = \frac{D}{\delta} \times \frac{S}{V} \times (Cs_{O2} - C_{O2}) \qquad (6)$$

467 where δ is the thickness of the diffusion layer, and is strongly dependent on stirring; D is the O_2
468 diffusion coefficient (1.83 cm^2 d^{-1}, Ploug, 2001); S is the surface of contact between air and
469 water (415.5 cm^2); V is the volume of the solution, which changed progressively during
470 sampling; and Cs_{O2} is the saturation concentration of the O_2 in seawater (229.9 μM). Using these
471 equations and parameters, we estimated the maximum δ above which the solution will be anoxic.
472 Considering that the risk of consuming all O_2 is greater for a larger volume of solution (with the
473 same surface area), we conservatively used the volume of solution at the beginning of the
474 experiment $V=V_0$ (8100 cm^3).

475 We seek a value of δ_{max}, at which $\frac{dC_{O2}}{dt}$ will always be positive when C_{O2} approaches 0 so that
476 the system can never go anoxic. This condition is met when

$$R_{loss} \leq R_{diff} = \frac{D}{\delta} \times \frac{S}{V} \times C_{SO2} \quad (7)$$

or whenever

$$\delta_{\max} = \frac{D}{R_{loss}} \times \frac{S}{V_0} \times Cs_{O2} \quad (8)$$

We calculated that when the volume is at its maximum in the flask (8100 cm^3 at the beginning of the experiment), the depth of the diffusive layer must be less than 0.1 cm for the solution to remain oxic. The thickness of the diffusion layer is 0.27 cm with no stirring and can be as small as 0.0015 cm when the stirring is intense (Gladyshev, 2002). Since our flasks were well mixed, it is very unlikely that O_2 was a limiting factor.

A second explanation is that degradation products built up in the flask and poisoned the bacteria (Westrich and Berner, 1984; Aller and Aller, 1998). We cannot exclude this possibility, but calculating kinetic parameters over only 25 days should alleviate some of this problem. This period of time is a reasonable compromise between the need to follow the degradation of *S. marinoi* as long as possible so as to better understand reactions in the water column and the risk of accumulating inhibiting metabolites. Finally, the bacteria might have stopped growing due to viral lysis, grazing or a lack of labile substrate fuelling their growth (Fig. 2).

4.2 Importance of Si-C interactions to $bSiO_2$ dissolution

Previous dissolution studies have assumed that the diatom frustule is composed of a single $bSiO_2$ phase (see review in Van Cappellen *et al.*, 2002b). Results from our modelling exercise suggest instead that the frustule of *S. marinoi* is composed of two phases of $bSiO_2$ with different dissolution characteristics. This idea, previously hypothesized by Kamatani and Riley (1979) from dissolution rate measurements and by Gallinari *et al.* (2002) from solubility equilibrium measurements, is consistent with the complexity of the frustule structure. During silicification, polyamines and silaffin proteins catalyze precipitation of organo-silicon particles

501 of different shape and structure that determine the morphology of different diatom species
502 (Kröger *et al.*, 2000; Hildebrand, 2003). As a result of these interactions, diatom frustules have a
503 complex 3-D structure and are shaped like an elliptic or cylindrical box. Each half is composed
504 of a valve and girdle bands that are built at different times in the cell cycle (Hildebrand and
505 Wetherbee, 2003). In our study we distinguish two $bSiO_2$ phases and calculate their dissolution
506 rate constants. Even though we didn't determine a direct relation between these dissolution
507 characteristics and the structure of the frustule, we were able to determine the impact of two-
508 phase dissolution on the organic matrix of the cells as discussed below (see section 4.3).
509 Diatom frustules include organic layers that consist mainly of sugars and amino acids
510 (Hildebrand *et al.*, 2006). The major amino acids in this coating are GLY, THR, and SER,
511 suggesting that bonding with silica occurs through SER and THR, using their OH groups (Hecky
512 *et al.*, 1973). GLY enrichment observed during our study in the refractory (second) $bSiO_2$ phase
513 might suggest a more important role of GLY. Si-C or Si-O-C interactions are thought to protect
514 silica from dissolution until the organic matrix is removed by bacteria (Hecky *et al.*, 1973;
515 Patrick and Holding, 1985; Bidle and Azam, 2001). The different dissolution parameters of the
516 $bSiO_2$ phases may be due to different associations between silica and organic compounds in
517 different sections of the frustule. Indeed, Abramson *et al.* (2008) observed changes in the
518 distribution of organic compounds inside the frustule that would support this argument. The very
519 slow dissolution rate constant for the second $bSiO_2$ phase could be due to protection by the
520 organic matrix. We suggest (1) that only a part of the $bSiO_2$ is protected by the organic coating,
521 and (2) that this protection lasts for a longer time than was previously thought. Low bacterial
522 concentration could also partially explain why the protection of the second $bSiO_2$ phase lasted so
523 long, while in previous studies the protection was only temporary. The linear correlation between
524 FFA and the total $bSiO_2$ indicates that these compounds are associated with both phases of
525 $bSiO_2$, even though all FFA were completely degraded while 31% of the $bSiO_2$ still remained.
526 Few FFA were associated with the intracellular pool of lipids. Because of their amphipathic

properties due to the carboxyl group bonded to the long carbon chain, FFA probably play a role in the organization of the organic matrix involved in building the frustule (Chevallard and Guenoun, 2006). The relationship between FFA degradation and dissolution of the two $bSiO_2$ phases, and the fact that FFA were completely degraded before the total dissolution of the $bSiO_2$, might also indicate another type of interaction, possibly adsorption of FFA on the silica surface.

In the present study, lipid classes and individual amino acids showed a general correlation with $bSiO_2$ concentration (Figs. 7 and 8). The modelling experiment showed that $bSiO_2$ and carbon pool degradation followed different patterns; they are represented in our model by different sets of equations. Moreover, in our in vitro experiment, external parameters like temperature were constant and can not be responsible for the relation observed in Figures 7 and 8. Thus we can safely suppose that a causal correlation exists between $bSiO_2$ dissolution and the amino acids or lipids degradation. The turnover of the portion of these organic compounds that is correlated with dissolution of either the first or second $bSiO_2$ phase (P1 and P3) was very slow compared to the degradation of the remaining pool of these compounds. For example, for the amino acids, the turnover of Si(1)-THAA and Si(3)-THAA was slow compared to the loss of THAA in general. This correlation suggests that there may exist a direct association between each $bSiO_2$ phase and the corresponding organic compounds (Si(1)-THAA, Si(3)-THAA, Si(1)-Lip and Si(2)-Lip). Since the amounts of Si-THAA and Si-TLip related to each phase were similar (~10-30 %), differences between $bSiO_2$ dissolution rate constants stem mainly from the compositions of the pools. Some membrane lipids mainly MGDG were mostly associated with the first $bSiO_2$ phase. DPG+PG still had high concentrations at the end of P2 when most degradation occurred. The second $bSiO_2$ phase was more strongly correlated with neutral lipid alcohols (ST and ALC) but also with membrane lipids DPG+PG and PE. In the first $bSiO_2$ phase, GLU, ASP, and LEU constituted most of the Si(1)-THAA pool and this phase contains no LYS at all. In contrast in the second $bSiO_2$ phase, Si(3)-THAA had a composition similar to the diatom's intracellular THAA, except for an increase of the GLY composition.

553 It is not clear whether differences in organic carbon content and/or different associations
554 between $bSiO_2$ and organic carbon in each of the two $bSiO_2$ phases explains the differences
555 between $bSiO_2$ dissolution rates and also between solubility equilibria. The organic matter that
556 makes up part of the diatom frustule helps strengthen the structure, thus increasing its resistance
557 to mechanical forces like those from grazers (Hamm *et al.*, 2003). The role of organic
558 compounds in silica dissolution is, however, more difficult to determine. In addition to the
559 bonds between silica and the OH moiety of SER or THR (Hecky *et al.*, 1973), silica particles are
560 linked to organic compounds by nitrogen bonds (Sumper and Kröger, 2004). Indeed, Gendron-
561 Badou *et al.* (2003) noted that Si-C and Si-N bonds are present in fresh diatoms while only Si-O-
562 Si and Si-O-R bonds are visible in fossilized diatoms. Different associations between silica and
563 organic compounds resist degradation and dissolution differently and may explain the
564 differences we observed between dissolution rate constants and solubility equilibria of the two
565 $bSiO_2$ phases.
566 The different dissolution rates of the two $bSiO_2$ phases might also be due to different
567 physico-chemical properties in the silica structure itself. In the presence of some sillafins, silica
568 precipitation of porous blocks has been observed in vitro; in contrast, when silica precipitation is
569 catalyzed by polyamines, spherical silica particles are formed (Sumper and Kröger, 2004). If the
570 first silica phase is more porous due to the presence of organic matter or due to the compounds
571 that catalyzed silica formation, the dissolution rate constant of this $bSiO_2$ will be higher (Van
572 Cappellen *et al.*, 2002a). Also, when the silica structure is chemically more organized (in mineral
573 form, as opposed to amorphous, like opal), dissolution rate and solubility are lower. Gendron-
574 Badou *et al.* (2003) determined that the structure of $bSiO_2$ from fossilized diatoms from
575 sediments is more organized than that of fresh diatom frustules due to condensation processes
576 that continue after they are deposited. It is also possible that fresh diatoms already have a more
577 organized phase, as suggested by the low dissolution rate (in the present study) and the low
578 solubility equilibrium (Gallinari *et al.*, 2002) of the second $bSiO_2$ phase. During dissolution, the

579 two different rate constants will cause an increase of the ratio of the more organized phase to the
580 amorphous phase.
581 The difference between dissolution rate constants and between solubility equilibria could
582 be due to chemical bonds between silica and organic matter or to structural characteristics of the
583 $bSiO_2$. In any case it may be closely linked to the presence of organic compounds either inside
584 the frustule itself or during the silicification process. This conclusion emphasizes the need to link
585 studies of carbon and silica production and recycling if we are to better understand both C and Si
586 cycles. The following section will accentuate this conclusion by showing the reverse: the
587 importance of $bSiO_2$ to carbon degradation.
588
589 **4.3 Si-C interactions and their role on carbon degradation**
590 $bSiO_2$ dissolution was best described by Model 2, while the turnover of each organic
591 compound investigated here was best fit by Model 1 or 3 (Fig. 5). The use of Model 3 to
592 describe compound turnover means that either (1) most organic compounds were present as two
593 pools of matter degrading one after the other or (2) degradation rate constants increased at some
594 point due to a change in environmental factors. In most cases the loss rate constant increased
595 (POC, PON, THAA, PE, and MGDG) or decreased (other lipid classes) when the dissolution of
596 the first $bSiO_2$ phase was almost complete, from which we conclude that the first $bSiO_2$ phase
597 must have influenced loss of organic matter.
598 Most of the ALC, PE and ST present in the intracellular pool of organic compounds
599 seems to have been protected by the first $bSiO_2$ phase, but due to the high variability of lipid
600 class behaviour the pattern for TLip is less clear than the one for THAA. THAA degradation is
601 consistent with the idea that Si(2)-THAA is encased within diatom frustules, and is released as
602 soon as the first $bSiO_2$ phase is completely removed. While several amino acids increased in
603 concentration between day 11 and day 20 (Fig. 6b), bacterial numbers peaked at day 13, which
604 corresponds to the THAA maximum (Fig. 1 and Fig. 2). However, bacterial carbon accounted

605 for only 0.2 to 2.4 ± 0.3 % of total carbon (Fig. 3). Bacterial biomass cannot account for the
606 increase of THAA, but the increase of bacterial number could be explained by this input of labile
607 organic carbon. Ingalls *et al.* (2003, 2006) measured Si-THAA (THAA bound and/or within
608 $bSiO_2$) obtained after complete dissolution of the $bSiO_2$ using successive treatments with 6N HCl
609 and HF. They found that Si-THAA made up 0.7-7 % of the total THAA in diatoms from
610 plankton tows and sediment trap samples. In our study, Si-THAA was a larger portion of total
611 THAA than in the studies of Ingalls *et al.* (2003, 2006). We define three pools of THAA: Si(1)-
612 THAA degradation is correlated to the dissolution of the first $bSiO_2$ phase; Si(2)-THAA is the
613 pool of THAA that are enclosed between the two $bSiO_2$ phases. Both of these pools were
614 protected by the first $bSiO_2$ phase. The third pool, Si(3)-THAA, is attached to the second phase
615 of the frustule; due to the low dissolution rate constant of this phase, it was protected for longer
616 time.

617 The composition of Si(2)-THAA is dominated by GLY and LYS, which are major
618 components of silaffins (Table 2). As part of the silicification process (Hildebrand, 2003;
619 Sumper and Kröger, 2004), these proteins are present in the silica deposition vesicles (SDV) that
620 become part of the diatom wall at the end of frustule formation (Martin-Jézéquel *et al.*, 2000).
621 Thus the Si(2)-THAA pool may be assembled during the silicification process, and may result
622 from the integration of the SDV's into the frustule. Similarity between most of the substitution
623 times *ts* listed in Table 4 and the release time of Si(2)-THAA suggests that k_2 represents the
624 degradation rate constant of this portion of THAA. After being released, Si(2)-THAA turned
625 over very fast (k_2 in Table 4). Most of these amino acids were completely dissolved or degraded
626 shortly after the total dissolution of the first $bSiO_2$ phase, which suggests that this pool of THAA
627 is not directly bound to $bSiO_2$. The high loss rate constant of Si(2)-THAA may suggest that this
628 pool of THAA was dissolved (chemical mechanism) rather than degraded (biological
629 mechanism) as soon as it was exposed. Another possible explanation to this fast turn over rate is
630 a change in degradation mechanism. During degradation, amino acids are released from protein

631 by enzymatic cleavage at the end of the proteins (exopeptidase) or in the middle of the
632 polypeptide chain (endopeptidase). If the proteins are opened up during the silicification process,
633 exopeptidases could act at both ends of the protein and degradation would be faster.
634 Due to their high turnover rate Si(2)-THAA may have been dissolved during the strong
635 HCl treatment or degraded before analysis in the study of Ingalls *et al.* (2003; 2006).
636 Accordingly, the quantification of Si-THAA made by Ingalls *et al.* (2003) might have only
637 targeted THAA bound to the second $bSiO_2$ phase of the frustule (Si(3)-THAA). The
638 composition of Si-THAA in Ingalls *et al.* (2003) is similar to our Si(3)-THAA except that LYS is
639 more abundant in Si(3)-THAA and GLY slightly less abundant (Table 2). The low solubility of
640 the second $bSiO_2$ phase is consistent with the increase in Si-THAA/THAA with depth in their
641 study.
642 The $bSiO_2$ protected from degradation the organic matter that was directly associated
643 with the frustule (Si(1)-THAA, Si(3)-THAA and Si-Lip). The first $bSiO_2$ phase also protected
644 the lipids (some DPG+PG) and amino acids (Si(2)-THAA) trapped inside the frustule possibly
645 between the 2 phases, as shown by the correlation curve (Figs. 7 and 8). Moreover, the sudden
646 increase in POC degradation rate (Fig. 1) after release of the trapped material is not associated
647 with an increase in bacterial concentration (Figs. 2 and 3) but with the end of the dissolution of
648 the first $bSiO_2$ phase. It is hardly a coincidence that the end of dissolution of the first $bSiO_2$
649 phase occurred exactly when the degradation of the POC, PON and THAA increased. The
650 mechanisms behind this observation are not clear yet; the dissolution of this phase probably gave
651 bacteria better access to the internal carbon of the cell, possibly because the integrity of the
652 frustule can not be maintained without the presence of the first $bSiO_2$ phase. This could happen
653 through increasing pores size as sometimes shown by pictures of diatom frustules during
654 dissolution, or because the box-shaped frustule opens at the end of the first $bSiO_2$ phase
655 dissolution as observed after sexual phases (Crawford 1995), both triggering cell lysis. In any
656 case we can safely conclude that the first $bSiO_2$ phase of the diatom frustule also protects most of

657 the intracellular carbon; at the end of the dissolution of the first $bSiO_2$ phase 69% of the POC
658 was still not degraded. Due to the very low dissolution rate of the second $bSiO_2$ phase, the
659 associated organic compounds (Si(3)-THAA and Si(2)-Lip) might be protected for a long period
660 of time; they would even be preserved in the sediment with the $bSiO_2$.

661 The presence of organic compounds inside the frustule and/or during silicification
662 determines the solubility of the different parts of the frustule. Moreover, intracellular carbon and
663 Si-bound organic compounds may be protected by at least some part of the frustule. These
664 reverse interactions prove that carbon and silica production and recycling must be studied in
665 parallel if we want to improve our understanding of mechanisms driving both POC and $bSiO_2$
666 sedimentation.

667

668 Acknowledgements

669 We are grateful to Annick Masson for her technical assistance with POC analyses. Thanks to
670 everyone in the LMGEM for their kindness and help during the experimental work. This work
671 was funded by the EU, partly through the ORFOIS (EVK2-CT2001-00100) project and partly
672 through the program Marie Curie, project CARBALIS (MOIF- CT-2006-022278). This is
673 contribution # 1081 of the IUEM and xxx of Stony Brook University. Support was also provided
674 by the MedFlux program of the U.S. NSF Chemical Oceanography division, and this is MedFlux
675 contribution No. XXX.

676

677

678

679 Bibliography

680 Abramson, L., Wirick, S., Lee, C., Jacobsen, C., Brandes, J.A, 2008. The use of soft X-ray
681 spectromicroscopy to investigate the distribution and composition of organic matter in a
682 diatom frustule and a biomimetic analog. Deep-Sea Research II, this volume.
683 Aller, R.C., Aller, J.Y., 1998. The effect of biogenic irrigation intensity and solute exchange on
684 diagenetic reaction rates in marine sediments. Journal of Marine Research 56, 905-936.
685 Armstrong, R.A., Lee, C., Hedges, J.I., Honjo, S., Wakeham, S.G., 2002. A new, mechanistic
686 model for organic carbon fluxes in the ocean based on the quantitative association of
687 POC with ballast minerals. Deep-Sea Research II 49, 219-236.
688 Berge, J.-P., Gouygou, J.-P., Dubacq, J.-P., Durand, P., 1995. Reassessment of lipid composition
689 of the diatom, *Skeletonema costatum*. Phytochemistry 39 (5), 1017-1021.
690 Bidle, K.D., Azam, F., 2001. Bacterial control of silicon regeneration from diatom detritus:
691 significance of bacterial ectohydrolases and species identity. Limnology and
692 Oceanography 46, 1606-1623.
693 Bligh, E.G., Dyer, W.J., 1959. A rapid method for total lipid extraction and purification.
694 Canadian Journal of Biochemistry and Physiology 37, 911-917.
695 Brzezinski, M.A., 1985. the Si:C:N ratio of marine diatoms: interspecific variability and the
696 effect of some environmental variables. Journal of Phycology 21, 347-357.
697 Chevallard, C., Guenoun, P., 2006. Les matériaux biomimétiques. Bulletin de la Societe
698 Française de Physique 155, 5-10.
699 Cowie, G.L., Hedges, J.I., 1996. Digestion and alteration of the biochemical constituents of a
700 diatom (*Thalassiosira weissflogii*) ingested by an herbivorious copepod (*Calanus*
701 *pacificus*). Limnology and Oceanography 41, 581-594.
702 Crawford RM, 1995. The role of sex in the sedimentation of a marine diatom bloom. Limnology
703 and Oceanography 40 (1), 200-204.
704 D'ippolito, G., Tucci, S., Cutignano, A., Romano, G., Cimino, G., Miralto, A., Fontana, A., 2004.
705 The role of complex lipids in the synthesis of bioactive aldehydes of the marine diatom
706 *Skeletonema costatum*. Biochimica et Biophysica Acta 1686, 100-107.
707 Dixit, S., Van Cappellen, P., Van Bennekom, A.J., 2001. Processes controlling solubility of
708 biogenic silica and porewater build up of silicic acid in marine sediments. Marine
709 Chemistry 73 (3-4), 333-352.
710 Engel, A., Abramson, L., Szlosek, J., Liu, Z., Stewart, G., Hirschberg, D., Lee, C, 2008.
711 Investigating the effect of ballasting by $CaCO_3$ in *Emiliania huxleyi*: II. Decomposition
712 of particulate organic matter. Deep-Sea Research part II, this volume.
713 Gallinari, M., Ragueneau, O., Corrin, L., Demaster, D.J., Tréguer, P., 2002. The importance of
714 water column processes on the dissolution properties of biogenic silica in deep sea-
715 sediments I. Solubility. Geochimica et Cosmochimica Acta 66 (15), 2701-2717.
716 Garvey M, Moriceau B, Passow U, 2007. Applicability of the FDA assay to determine the
717 viability of marine phytoplankton under different environmental conditions. Mar Ecol
718 Prog Ser 352, 17-26.
719 Gehlen, M., Bopp, L., Emprin, N., Aumont, O., Heinze, C., Ragueneau, O., 2006. Reconciling
720 surface ocean productivity, export fluxes and sediment composition in a global
721 biogeochemical ocean model. Biogeosciences Discussion 3, 803-836.
722 Gendron-Badou, A., Coradin, T., Maquet, J., Fröhlich, F., Livage, J., 2003. Spectroscopic
723 characterization of biogenic silica. Journal of non-Crystalline Solids 316, 331-337.
724 Gladyshev, M.I., 2002. Biophysics of the surface Microlayer of Aquatic Ecosystems. IWA
725 Publishing, Cornwall, UK.
726 Gordon, L.I., Jennings, J.C., Ross, A.A., Krest, J.M., 1993. A suggested protocol for continuous
727 flow automated analysis of seawater nutrients. Technical report N° 93-1, OSU College of
728 Oceanography Descriptive, Corvallis, pp. 1-55.

729 Goutx, M., Wakeham, S.G., Lee, C., Duflos, M., Guigue, C., Liu, Z., Moriceau, B., Sempere, R.,
730 Tedetti, M., Xue, J., 2007. Composition and degradation of marine particles with
731 different settling velocities in the Northwestern Mediterranean sea. Limnology and
732 Oceanography 52 (4), 1645-1664.
733 Greenwood, J., Truesdale, V.W., Rendell, A.R., 2001. Biogenic silica dissolution in seawater - in
734 vitro chemical kinetics. Progress in Oceanography 48, 1-23.
735 Guillard, R.R.L., 1975. Culture of phytoplankton for feeding marine invertebrates. In: Smith,
736 W.L., Chanley, M.H. (Eds.), Culture of Marine Invertebrate Animals. Plenum Press, New
737 York, pp. 26-60.
738 Guillard, R.R.L., Ryther, J.H., 1962. Studies of marine planktonic diatoms. I. Cyclotella nana
739 Hustedt and Detonula confervacae (Cleve). Gran Can J Microbiol 8, 229-239.
740 Hamm, C.E., Merkel, R., Springer, O., Jurkojc, P., Maier, C., Prechtel, K., Smetacek, V., 2003.
741 Architecture and material properties of diatom shells provide effective mechanical
742 protection. Nature 421, 841-843.
743 Harvey, H.R., Tuttle, J.H., Bell, J.T., 1995. Kinetics of phytoplankton decay during simulated
744 sedimentation: Changes in biochemical composition and microbial activity under oxic
745 and anoxic conditions. Geochimica et Cosmochimica Acta 59 (16), 3367-3377.
746 Hecky, R.E., Mopper, K., Kilham, P., Degens, E.T., 1973. The amino acids and Sugar
747 Composition of Diatom Cell-Walls. Marine Biology 19, 323-331.
748 Hedges, J.I., Baldock, J.A., Gélinas, Y., Lee, C., Meterson, M., Wakeham, S.G., 2001. Evidence
749 for non -selective preservation of organic matter in sinking marine particles. Nature 409,
750 801-804.
751 Hilborn R, Mangel M, 1997. The ecological detective : Confronting Models with Data. In: Levin
752 SA, Horn HS (eds). Princeton University Press, New Jersey, USA, pp 315.
753 Hildebrand, M., 2003. Biological processing of nanostructured silica in diatoms. Progress in
754 Organic Coatings 47, 256-266.
755 Hildebrand, M., Wetherbee, R., 2003. Components and control of silicification in diatoms. In:
756 Mueller, W.E.G. (Ed.) Silicon Biomineralization: Biology, Biochemestry, Molecular
757 Biology, Biotechnology. Springer, New York, pp. 11-57.
758 Hildebrand, M., York, E., Kelz, J.I., Davis, A.K., Frigeri, L.G., Allison, D.P., Doktycz, M.J.,
759 2006. Nanoscale control of silica morphology and three-dimensional structure during
760 diatom cell wall formation. Journal of Materials Research 21 (10), 2689-2698.
761 Ingalls, A.E., Lee, C., Wakeham, S.G., Hedges, J.I., 2003. The role of biominerals in the sinking
762 flux and preservation of amino acids in the Southern Ocean along 170°W. Deep-Sea
763 Research II 50, 713-738.
764 Ingalls, A.E., Liu, Z., Lee, C., 2006. Seasonal trends in the pigments and amino acid
765 compositions of sinking particles in biogenic CaCO3 and SiO2 dominated regions of the
766 Pacific sector of the Southern Ocean along 170°W. Deep-Sea Research Part I:
767 Oceanographic Research Papers 53 (5), 886-859.
768 Jin, X., Gruber, N., Dunne, J.P., Sarmiento, J.L., Armstrong, R.A., 2006. Diagnosing the
769 contribution of phytoplankton functional groups to the production and export of
770 particulate organic carbon, CaCO3, and opal from global nutrient and alkalinity
771 distributions. Global Biogeochemical Cycles 20. doi:10.1029/2005GB002532.
772 Kamatani, A., 1982. Dissolution Rates of silica from diatoms decomposing at various
773 temperature. Marine Biology 68, 91-96.
774 Kamatani, A., Riley, J.P., 1979. Rate dissolution of diatom silica walls in seawater. Marine
775 Biology 55, 29-35.
776 Kamatani, A., Riley, J.P., Skirrow, G., 1980. The dissolution of opaline silica of diatom tests in
777 seawater. Journal of the Japanese Oceanographic Society 36, 201-208.

778 Kröger, N., Deutzmann, R., Bergsdorf, C., Sumper, M., 2000. Species-specific polyamines from
779 diatoms control silica morphology. Proceedings of the National Academy of Sciences of
780 the United States of America 97, 14133-14138. doi:10.1073/pnas.260496497.
781 Lavens, P., Sorgeloos, P. (Eds.), 1996. Manual on the production and use of live food for
782 aquaculture, Rome.
783 Lee, B.-G., Fisher, N.S., 1992. Degradation and elemental release rates from phytoplankton
784 debris and their geochemical implications. Limnology and Oceanography 37 (7), 1345-
785 1360.
786 Lee, C., Cronin, C., 1982. The vertical flux of particulate organic nitrogen in the sea:
787 Decomposition of amino acids in the Peru upwelling area and the equatorial Atlantic.
788 Journal of Marine Research 41, 227-251.
789 Lee, C., Wakeham, S.G., Hedges, J.I., 2000. Composition and flux of particulate amino acids
790 and chloropigments in equatorial Pacific seawater and sediments. Deep-Sea Research I
791 47, 1535-1568.
792 Lee, C., Wakeham, S.G., Peterson, M.L, Cochran, J.K., Miquel, J.C., Armstrong, R.A., Fowler,
793 S., Hirschberg, D., Beck, A., Xue, J, 2008. Particulate matter fluxes in time-series and
794 settling velocity sediment traps in the northwestern Mediterranean Sea. Deep-Sea
795 Research II, this volume.
796 Liu, Z., Lee, C., Wakeham, S.G., 2006. Effects of mercuric chloride and protease inhibitors on
797 degradation of particulate organic matter from the diatom *Thalassiosira pseudonana*.
798 Organic Geochemistry 37, 1003-1018.
799 Martin-Jézéquel, V., Hildebrand, M., Brzezinski, M.A., 2000. Silicon metabolism in diatoms:
800 implications for growth. Journal of Phycology 36, 821-840.
801 Moriceau, B., Soetaert, K., Gallinari, M., Ragueneau, O., 2007. Importance of particle dynamics
802 on reconstructed water column biogenic silica fluxes. Global Biogeochemical Cycles in
803 press.
804 Mullin, J.B., Riley, J.P., 1965. The spectrophotometric determination of silicate-silicon in natural
805 waters with special reference to seawater. Analytica Chimica Acta 46, 491-501.
806 Nelson, D.M., Tréguer, P., Brzezinski, M.A., Leynaert, A., Quéguiner, B., 1995. Production and
807 dissolution of biogenic silica in the ocean: Revised global estimates, comparison with
808 regional data and relationship to biogenic sedimentation. Global Biogeochemical Cycles
809 9 (3), 359-372.
810 Parrish, C.C., 1988. Dissolved and particulate marine lipid classes: a review. Marine Chemistry
811 23, 17-40.
812 Patrick, S., Holding, A.J., 1985. The effect of bacteria on the solubilization of silica in diatom
813 frustules. Journal of Applied Bacteriology 59, 7-16.
814 Ploug, H., 2001. Small-scale oxygen fluxes and remineralization in sinking aggregates.
815 Limnology and Oceanography 46 (7), 1624-1631.
816 Porter, K.G., Feig, Y.S., 1980. The Use of DAPI for Identifying and Counting Aquatic
817 Microflora. Limnology and Oceanography 25 (5), 943-948.
818 Ragueneau, O., Dittert, N., Pondaven, P., Tréguer, P., Corrin, L., 2002. Si/C decoupling in the
819 world ocean: is the Southern Ocean different? Deep-Sea Research II 49, 3127-3154.
820 Ragueneau, O., Tréguer, P., 1994. Determination of biogenic silica in coastal waters:
821 applicability and limits of the alkaline digestion method. Marine Chemistry 45, 43-51.
822 Rousseau, V., Leynaert, A., Daoud, N., Lancelot, C., 2002. Diatom succession, silicification and
823 silicic acid availability in Belgian coastal waters (Southern North Sea). Marine Ecology
824 Progress Series 236, 61-73.
825 Sempéré, R., Dafner, E., Van Wambeke, F., Lefèvre, D., Magen, C., Allègre, S., Bruyant, F.,
826 Bianchi, M., Prieur, L., 2003. Distribution and cycling of total organic carbon across the
827 Almeria-Oran Front in the Mediterranean Sea: Implications for carbon cycling in the
828 western basin. Journal of Geophysical Research 108 (C11). doi:10.1029/2002JC001475.

829 Sohrin, R., Sempéré, R., 2005. Seasonal variation in total oranic carbon in the northeast Atlantic
830 in 2000-2001. Journal of Geophysical Research 110 (C10S90).
831 doi:10.1029/2004JC002731.
832 Striby, L., Lafont, R., Goutx, M., 1999. Improvement in the Iatroscan thin-layer
833 chromatography-flame ionisation detection analysis of marine lipids. Separation and
834 quantitation of mono-and diacylglycerols in standards and natural samples. Journal of
835 Chromatography A 849, 371-380.
836 Sumper, M., Kröger, N., 2004. Silica formation in diatoms: the function of long-chain
837 polyamines and silaffins. Journal of Materials Chemistry 14, 2059-2065.
838 doi:10.1039/b401028k.
839 Tamburini, C., Garcin, J., Grégori, G., Leblanc, K., Rimmelin, P., Kirchman, D.L., 2006.
840 Pressure effects on surface Mediterranean prokaryotes and biogenic silica dissolution
841 during a diatom sinking experiment. Aquatic Microbial Ecology 43 (3), 267-276.
842 Tamburini, C., Goutx, M., Guigue, C., Garel, M., Lefèvre, D., Charrière, B., Sempéré, R., Pepa,
843 S., Peterson, M.L., Wakeham, S., Lee, C., 2008. Microbial alteration of sinking fecal
844 pellets: Effects of a continuous increase in pressure that simulates descent in the water
845 column. Deep-Sea Research II, this volume.
846 Tréguer, P., Le Corre, P., 1975. Manuel d'analyse des sels nutritifs dans l'eau de mer: utilisation
847 de l'auto-analyseur Technicon II. Université de Bretagne Occidentale, Brest.
848 Tréguer, P., Nelson, D.M., Bennekom, A.J.V., Demaster, D.J., Leynaert, A., Quéguiner, B.,
849 1995. The silica Balance in the World Ocean: A Reestimate. Science 268, 375-379.
850 Van Cappellen, P., Dixit, S., Gallinari, M., 2002a. Biogenic silica dissolution and the marine Si
851 cycle: kinetics, surface chemistry and preservation. Océanis 28 (3-4), 417-454.
852 Van Cappellen, P., Dixit, S., Van Beusekom, J., 2002b. Biogenic silica dissolution in the oceans:
853 Reconciling experimental and field-based dissolution rates. Global Biogeochemical
854 Cycles 16 (4), 1075, doi:10.1029/2001GB001431,2002.
855 Westrich, J.T., Berner, R.A., 1984. The role of sedimentary organic matter in bacterial sulfate
856 reduction: The G model tested. Limnology and Oceanography 29 (2), 236-249.
857
858

859

860 Figure legends

861 Fig. 1. Changes in the relative concentrations of POC (closed black diamonds), $bSiO_2$
862 (open diamonds), THAA (closed grey squares) and TLip (closed grey triangles) during the
863 degradation of *S. marinoi* in the dark at 20°C during the first 25 days of the experiment. The
864 concentrations relative to initial values are on a logarithmic scale.

865 Fig. 2. Change in total bacterial concentration over time during the 102-day degradation
866 experiment.

867 Fig. 3. Change in algal TOC (open circles), DOC (open diamonds), POC (closed squares)
868 and bacterial carbon (closed circles) with time during the degradation experiment.

869 Fig. 4. Change in the concentration of (a) 6 of the 8 lipid classes in μmol C L^{-1} relative to
870 TLip concentrations in μmol C L^{-1} (b) 9 of the 14 individual amino acids in μmol AA L^{-1}
871 relative to THAA in units of μmol AA L^{-1}, over time during the first 25 days of the 102-days
872 degradation experiment. Note that due to the low number of C atoms in GLY, the GLY peak in
873 μmol AA L^{-1} is more visible than if using μmol C L^{-1}.

874 Fig. 5. Model comparisons (a) Dissolution of $bSiO_2$. In this experiment, $bSiO_2$ is the only
875 compound whose loss is best represented by Model 2. Δ log(L) between Model 2 and Model 3
876 is 13. Period 1 is the period of time corresponding to the dissolution of 85% of the first $bSiO_2$
877 phase and 10% of the second $bSiO_2$ phase. During period 2, the last 15% of the first $bSiO_2$
878 dissolved and 10% more of the second $bSiO_2$ phase dissolved. In Period 3 only the second
879 $bSiO_2$ phase dissolved as less than 1.5% of the first $bSiO_2$ phase remained. (b) The curve depicts
880 the loss of POC (or any organic compound) with a dissolution or degradation rate constant that
881 increases with the *ts*. Model 1 fits the curve using C_0 = 8297 μmol C L^{-1} and k = 0.047 d^{-1} with a
882 likelihood log(L) = 98.7. Model 2 fits the model with the same likelihood using the same
883 parameters, i.e. $C_1 + C_2$ = 8297 μmol C L^{-1}, $k_1 = k_2$ = 0.047 d^{-1}. Model 3 give the best fit

884 ($\log(L) = 174.7$) using $C_0 = 7614$ µmol C L^{-1}, $ts = 10$ d, $k_1 = 0.025\,d^{-1}$ and $k_2 = 0.082\,d^{-1}$. This
885 example clearly shows that only Model 3 can depict accurately the loss when the rate constant
886 increases at some point in the experiment. Moreover, Model 2 never gives a better likelihood
887 than Model 1 under these conditions.

888 Fig. 6. Change in organic compound concentrations with time during the degradation of *S.*
889 *marinoi*. For clarity, 7 of the 8 lipid class concentrations in µmol Cl_{ip} L^{-1} over time are shown
890 (5a) and only 10 of the 14 amino acids in µmol AA L^{-1} over time (5b). Results depicted are only
891 for the first 25 days. Note that THAA concentrations are in µmol AA L^{-1}.

892 Fig. 7. Si-TLip interactions during the degradation of the *S. marinoi*. (a) Correlation
893 between the concentrations of the dissolved $bSiO_2$ from the first phase relative to its initial
894 concentration (estimated by the model) and each lipid class relative to its initial concentration.
895 (b) Correlation between concentration of the dissolved $bSiO_2$ from the second phase relative to
896 its initial concentration (estimated by the model) and each lipid class relative to its initial
897 concentration. Period 1 is the period of time corresponding to the dissolution of 85% of the first
898 $bSiO_2$ phase and 10% of the second $bSiO_2$ phase. During period 2, the last 15% of the first
899 $bSiO_2$ dissolved, and 10% more of the second $bSiO_2$ phase dissolved. In Period 3 only the
900 second $bSiO_2$ phase dissolved as less than 1.5% of the first $bSiO_2$ phase remained.

901 Fig. 8. Si-THAA interactions during the degradation of *S. marinoi*. (a) Correlation
902 between the concentration of the dissolved $bSiO_2$ from the first phase relative to its initial
903 concentration (estimated by the model) and individual THAA concentrations relative to their
904 initial concentrations. (b) Correlation between concentration of the dissolved $bSiO_2$ from the
905 second phase relative to its initial concentration (estimated by the model) and individual THAA
906 concentrations relative to their initial concentrations. The periods shown are the same as in Fig.
907 7.

908

909 Table 1: List of abbreviations used in the text to refer to organic and inorganic compounds

910 measured during the degradation experiment.

Biogenic Silica	$bSiO_2$	**Total Organic Carbon**	TOC
Silicic acid	dSi	**Particulate organic carbon**	POC
Particulate organic nitrogen	PON	**Dissolved Organic carbon**	DOC
Total Lipid classes	TLip	**Total Hydrolyzed Amino Acids**	THAA
Alcohols	ALC	Alanine	ALA
Di- and monophosphatidyl glycerides	DPG+PG	Arginine	ARG
		Aspartic acid	ASP
Free fatty acids	FFA	Glutamic acid	GLU
Monogalactosyldiglycerides	MGDG	Glycine	GLY
Monoglycerides	MG	Histidine	HIS
Phosphatidylethanolamines	PE	Isoleucine	ILE
Pigments	PIG	Leucine	LEU
Sterols	ST	Lysine	LYS
		Methionine	MET
		Phenylalanine	PHE
		Serine	SER
		Threonine	THR
		Tyrosine	TYR
		Valine	VAL
		γ-Aminobutyric acid	GABA

911

912 Table 2: Concentration in μmol C L^{-1} and composition in mole% of the different pools of THAA
913 in *S. marinoi*. The THAA row shows the initial concentration and composition of THAA before
914 dissolution began and does not include Si-THAA. Si(1)-THAA is the pool associated with the
915 first $bSiO_2$ phase, Si(2)-THAA is the pool of THAA enclosed between the $bSiO_2$ phases and
916 Si(3)-THAA is the pool associated with the second $bSiO_2$ phase.

THAA	ALA	ARG	ASP	GLU	GLY	HIS	ILE	LEU	LYS	PHE	SER	THR	TYR	VAL	TOT
THAA	105	223	318	379	139	59	174	317	187	260	128	136	170	174	2769
% THAA / THAAtot	4%	8%	11%	14%	5%	2%	6%	11%	7%	9%	5%	5%	6%	6%	
Si(1)-THAA	20	31	122	143	12	12	48	92	0	63	16	29	58	45	691
% Si(1)-THAA/ Si(1)-THAAtot	3%	5%	19%	22%	2%	2%	7%	14%	0%	10%	2%	5%	9%	7%	
Si(2)-THAA	9	0	52	37	92	17	21	19	96	21	0	12	18	21	332
% Si(2)-THAA/ Si(2)-THAAtot	2%	0%	13%	9%	23%	4%	5%	5%	24%	5%	0%	3%	5%	5%	
Si(3)-THAA	20	28	51	64	72	20	26	43	53	35	29	30	26	26	523
% Si(3)-THAA/ Si(3)-THAAtot	4%	5%	10%	12%	14%	4%	5%	8%	10%	7%	5%	6%	5%	5%	

917

Table 3: Concentration in µmol C L^{-1} and composition in mole% of the different lipid class in *S. marinoi*. The lipid row shows the initial concentration and composition of lipid before dissolution began and does not include Si-lipid. Si(1)-Lip is the pool associated with the first $bSiO_2$ phase, Si(2)-Lip is the pool of THAA associated with the second $bSiO_2$ phase.

Lipid class	**ALC**	**DPG+PG**	**FFA**	**MG**	**MGDG**	**PE**	**PIG**	**ST**	**total**
Lipids	30	98	366	104	189	44	604	40	1475
lipid class/ total lipid	2%	7%	25%	7%	13%	3%	41%	3%	
Si(1)-Lip	0	0-36	180-201	15-25	0	1-19	NC	1-11	386-469
Si(1)-Lip/ tot Si(1)-Lip	0%	0-8%	43-47%	4-5%	41-49%	0-4%		0-2%	
Si(2)-Lip	0-4	40-69	3	0	0	7-13	NC	9-20	125-175
Si(2)-Lip/ tot Si(2)-Lip	0-2%	32-39%	39-55%	0%	0%	6-7%		7-11%	

NC: No correlation

923

924 Table 4: Kinetic parameters and likelihood (log(L)) calculated by the 3 models. C_0 is the initial
925 concentration of the compound. C_1 and C_2 are the initial concentrations of the two phases (for
926 $bSiO_2$) or the two pools (organic compounds). k is the degradation/dissolution rate constant
927 calculated with Model 1. k_1 and k_2 are degradation/dissolution rate constants of C_1 and C_2 in
928 Model 2, respectively, or used before and after the substitution time ts in Model 3, respectively.
929 The last column indicates which model has been chosen in this study to determine the
930 degradation/dissolution rate constant and the initial concentration of each compound. For
931 compounds, see abbreviations table (Table 1).

	Model 1			**Model 2**					**Model 3**					Best Model fit
	C_0	k	log(L)	C_1	C_2	k_1	k_2	log(L)	C_0	ts	k_1	k_2	log(L)	
PON	1499	0.050	*98.5*	26	1473	0.051	0.051	*98.5*	1364	12	0.030	0.094	*135.6*	III
POC	8297	0.047	*98.7*	6884	1412	0.047	0.047	*98.7*	7614	10	0.025	0.082	*174.7*	III
$bSiO_2$	591	0.030	*70.7*	209	462	0.268	0.016	*109.0*	658	6	0.063	0.019	*97.7*	II
TLip	1232	0.033	*27.9*	704	724	0.014	0.100	*43.5*	1420	17	0.048	0.010	*44.9*	III
ALC	44	0.080	*9.2*	46	5	0.122	0.001	*10.1*	52	19	0.099	0.001	*13.5*	III
FFA	297	0.104	*21.8*	139	207	0.068	0.214	*23.1*	330	15	0.125	0.077	*25.0*	I
MG	97	0.045	*24.5*	21	85	0.497	0.033	*25.0*	107	5	0.094	0.036	*25.5*	I
MGDG	199	0.145	*9.0*	93	107	0.145	0.145	*9.0*	189	2	0.078	0.520	*19.6*	III
PE	54	0.097	*22.3*	51	3	0.097	0.097	*22.3*	42	6	0.016	0.119	*26.6*	III
PG+DPG	69	0.011	*17.9*	55	13	0.011	0.011	*17.9*	65	16	0.001	0.054	*19.0*	I
PIG	641	0.012	*29.7*	32	610	0.012	0.012	*29.7*	627	5	0.000	0.016	*30.4*	I
ST	41	0.031	*30.0*	11	30	0.031	0.031	*30.0*	35	13	0.001	0.080	*38.3*	III
THAA	3599	0.080	*32.9*	1903	1696	0.080	0.080	*32.9*	3137	13	0.054	0.139	*42.8*	III
ALA	132	0.070	*42.3*	31	102	0.073	0.073	*42.3*	117	12	0.048	0.120	*54.1*	III
ARG	339	0.113	*26.6*	39	300	0.113	0.113	*26.6*	243	9	0.024	0.175	*54.3*	III
ASP	419	0.100	*24.5*	312	107	0.100	0.100	*24.5*	324	5	0.001	0.121	*29.1*	III
GLU	454	0.080	*39.2*	23	431	0.080	0.080	*39.2*	405	13	0.065	0.147	*50.5*	III
GLY	172	0.045	*24.9*	67	105	0.045	0.045	*24.9*	147	16	0.015	0.182	*39.3*	III
HIS	73	0.063	*28.9*	44	29	0.063	0.063	*28.9*	65	16	0.039	0.167	*38.6*	III
ILE	223	0.082	*34.4*	210	13	0.082	0.082	*34.4*	192	12	0.050	0.137	*44.8*	III
LEU	413	0.090	*34.0*	117	299	0.091	0.091	*34.0*	348	12	0.050	0.150	*48.2*	III
LYS	268	0.068	*18.1*	181	88	0.068	0.068	*18.1*	223	14	0.031	0.170	*26.1*	III
PHE	336	0.083	*31.6*	332	4	0.083	0.083	*31.6*	280	12	0.040	0.148	*45.8*	III
SER	162	0.075	*42.6*	21	140	0.075	0.075	*42.6*	135	5	0.007	0.090	*49.7*	III
THR	165	0.064	*43.1*	17	149	0.064	0.064	*43.1*	151	13	0.045	0.110	*51.1*	III
TYR	185	0.068	*48.3*	157	28	0.068	0.068	*48.3*	187	21	0.070	0.012	*49.3*	I
VAL	219	0.076	*37.9*	179	39	0.076	0.076	*37.9*	194	12	0.050	0.124	*46.5*	III

932

933 Fig. 1

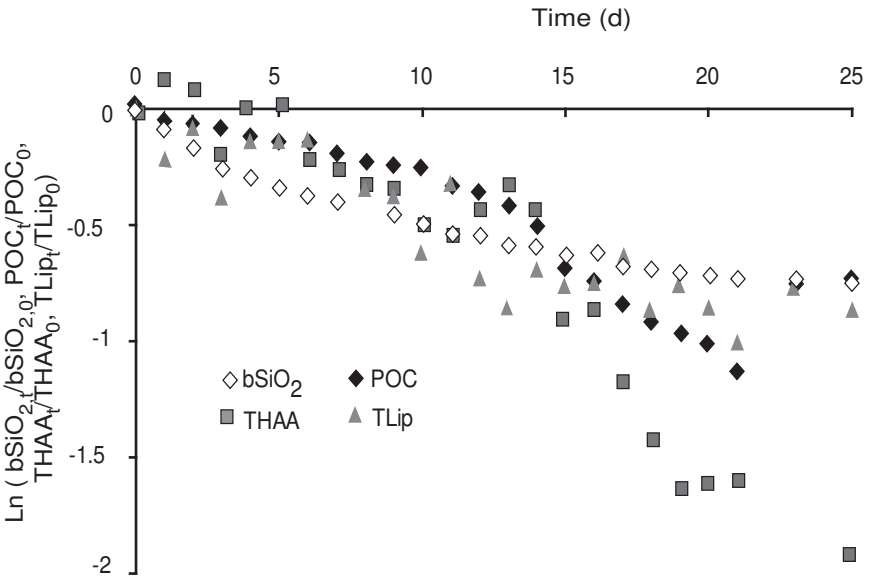
Time (d)
0
5
10
15
20
25
0
-0.5
-1
-1.5
-2
Ln (bSiO2t/bSiO2,0; POCt/POC0, THAAt/THAA0, TLipt/TLip0)
bSiO2
POC
THAA
TLip

934

935

936

937 Fig. 2

938

939

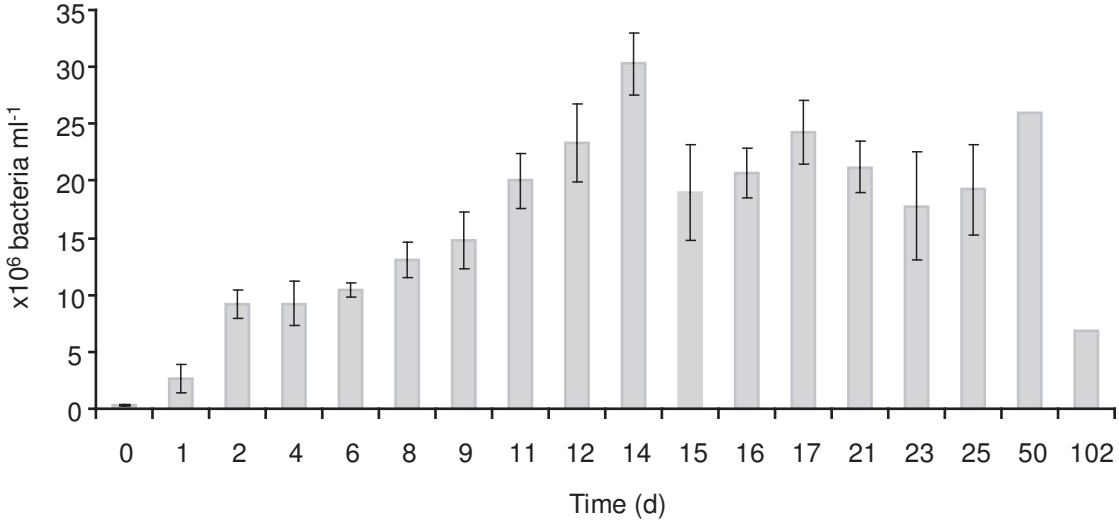

940

941

942

943

944

945 Fig. 3

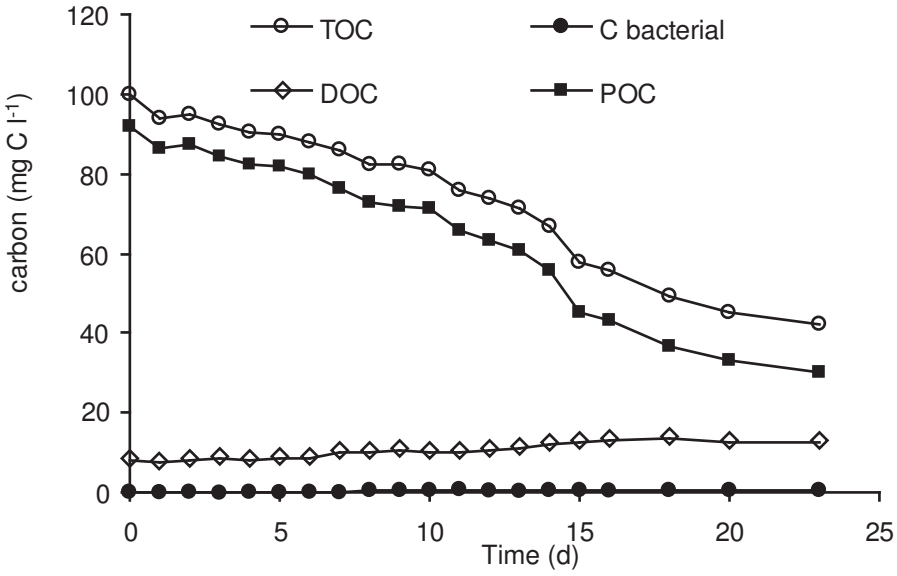

946

947 Fig. 4

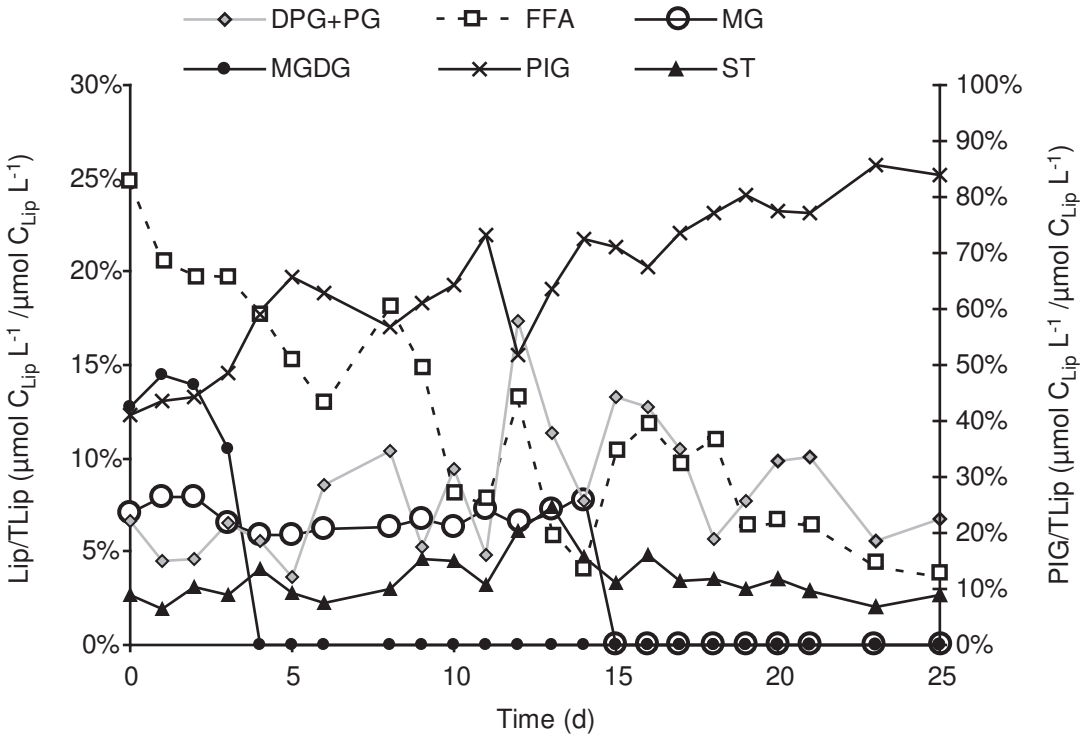
DPG+PG
FFA
MG
MGDG
PIG
ST
Lip/TLip (µmol C_Lip L-1 /µmol C_Lip L-1)
PIG/TLip (µmol C_Lip L-1 /µmol C_Lip L-1)
Time (d)

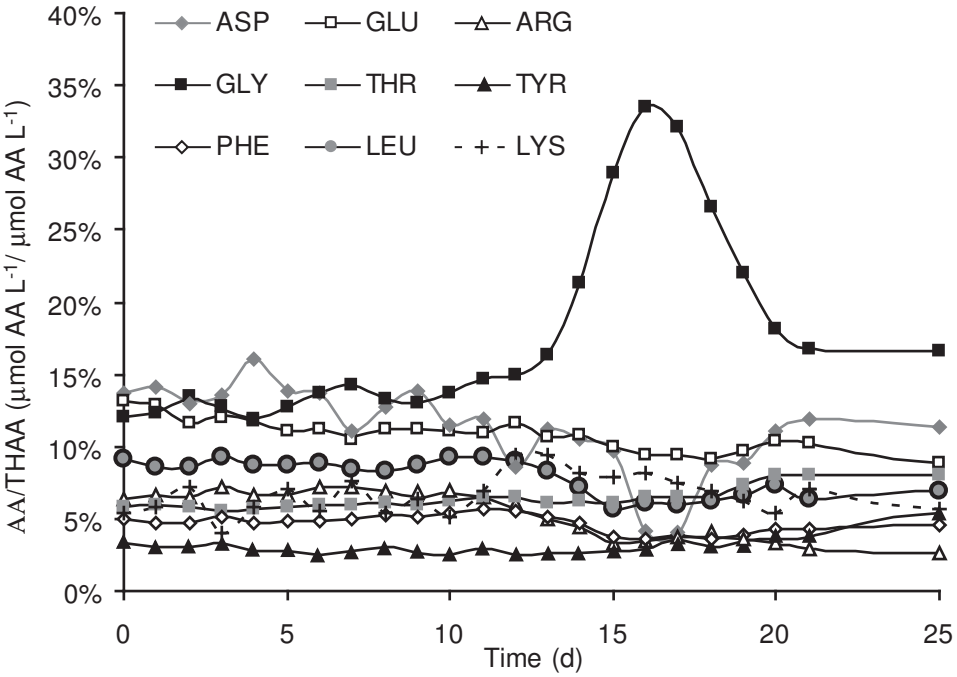
ASP
GLU
ARG
GLY
THR
TYR
PHE
LEU
LYS
AA/THAA (µmol AA L-1/ µmol AA L-1)
Time (d)

948

949

950 Figure 5:

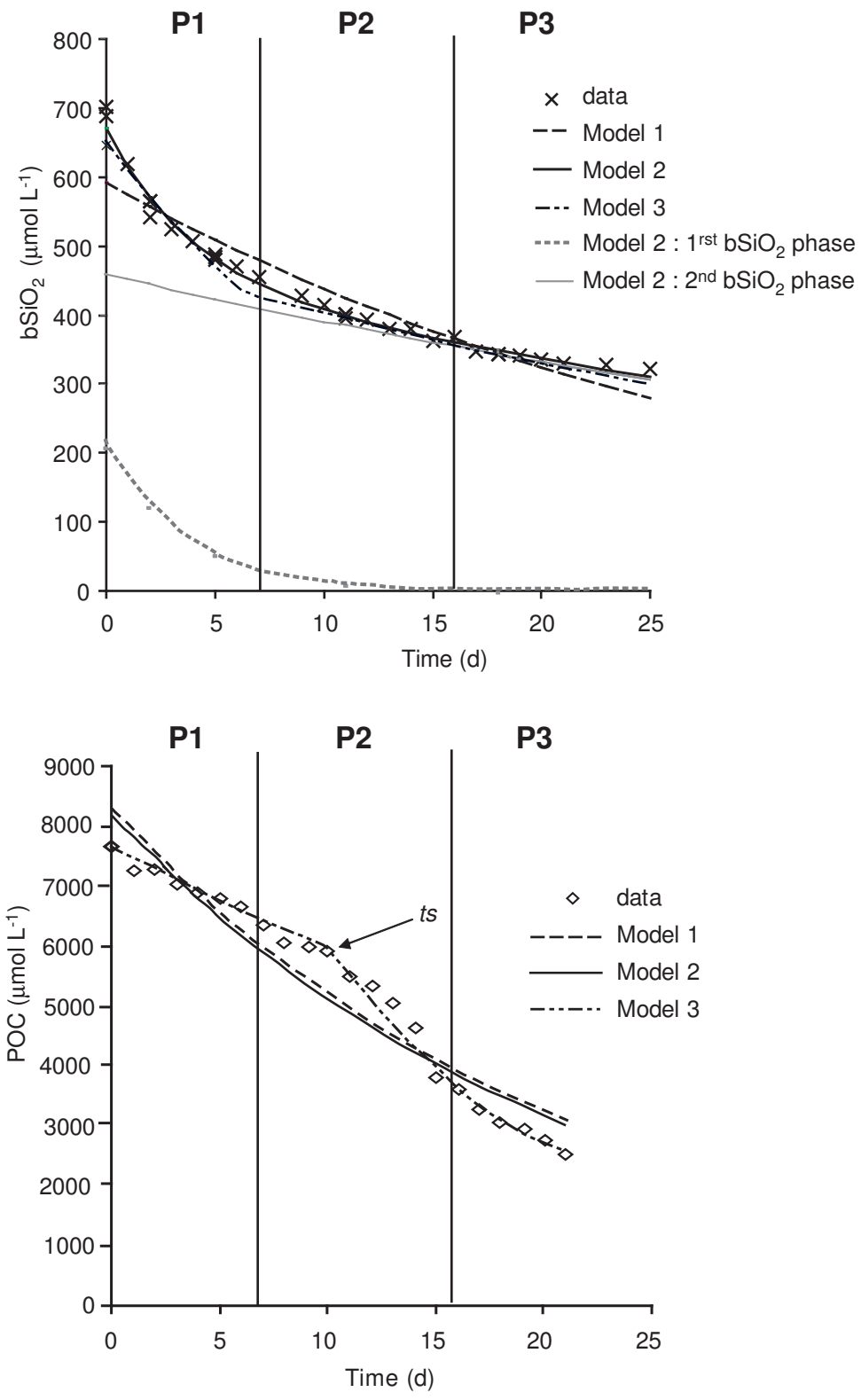

951

952 Fig. 6:

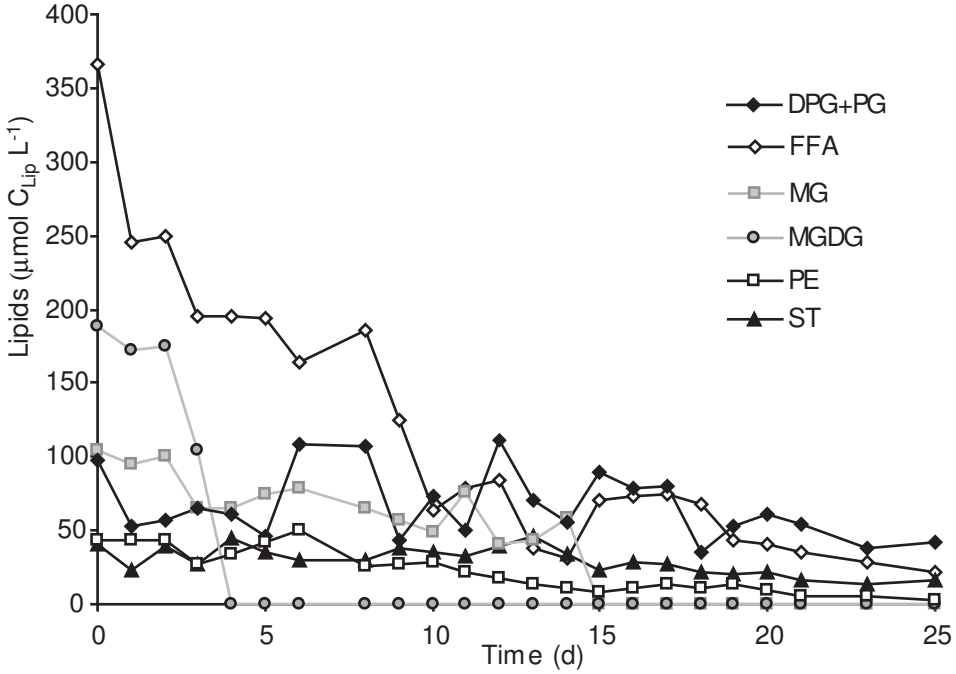
Lipids (µmol C_{Lip} L^{-1})
Time (d)
DPG+PG
FFA
MG
MGDG
PE
ST

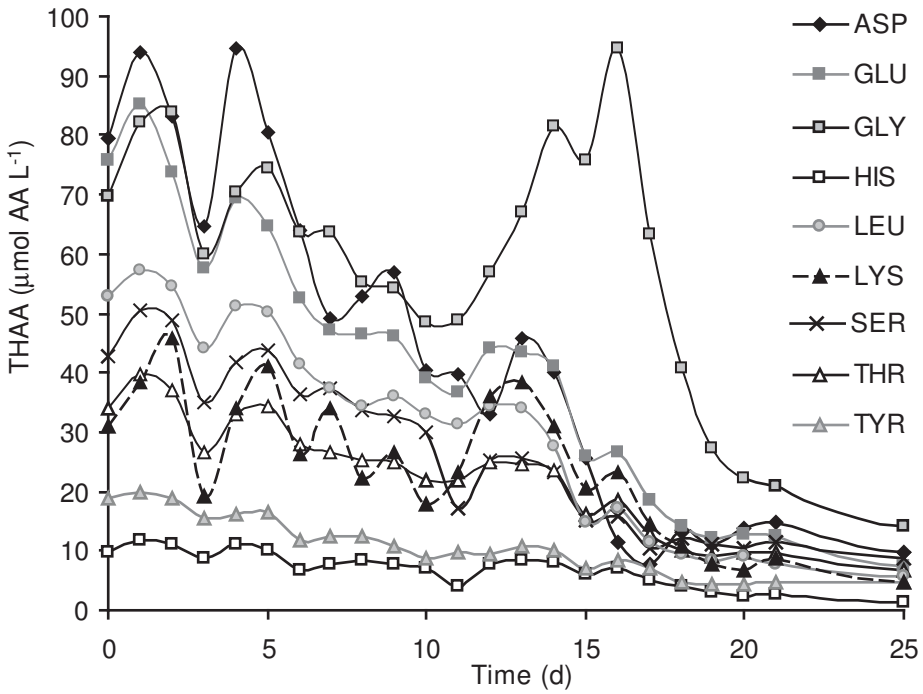
THAA (µmol AA L^{-1})
Time (d)
ASP
GLU
GLY
HIS
LEU
LYS
SER
THR
TYR

953

954

955 Fig. 7:

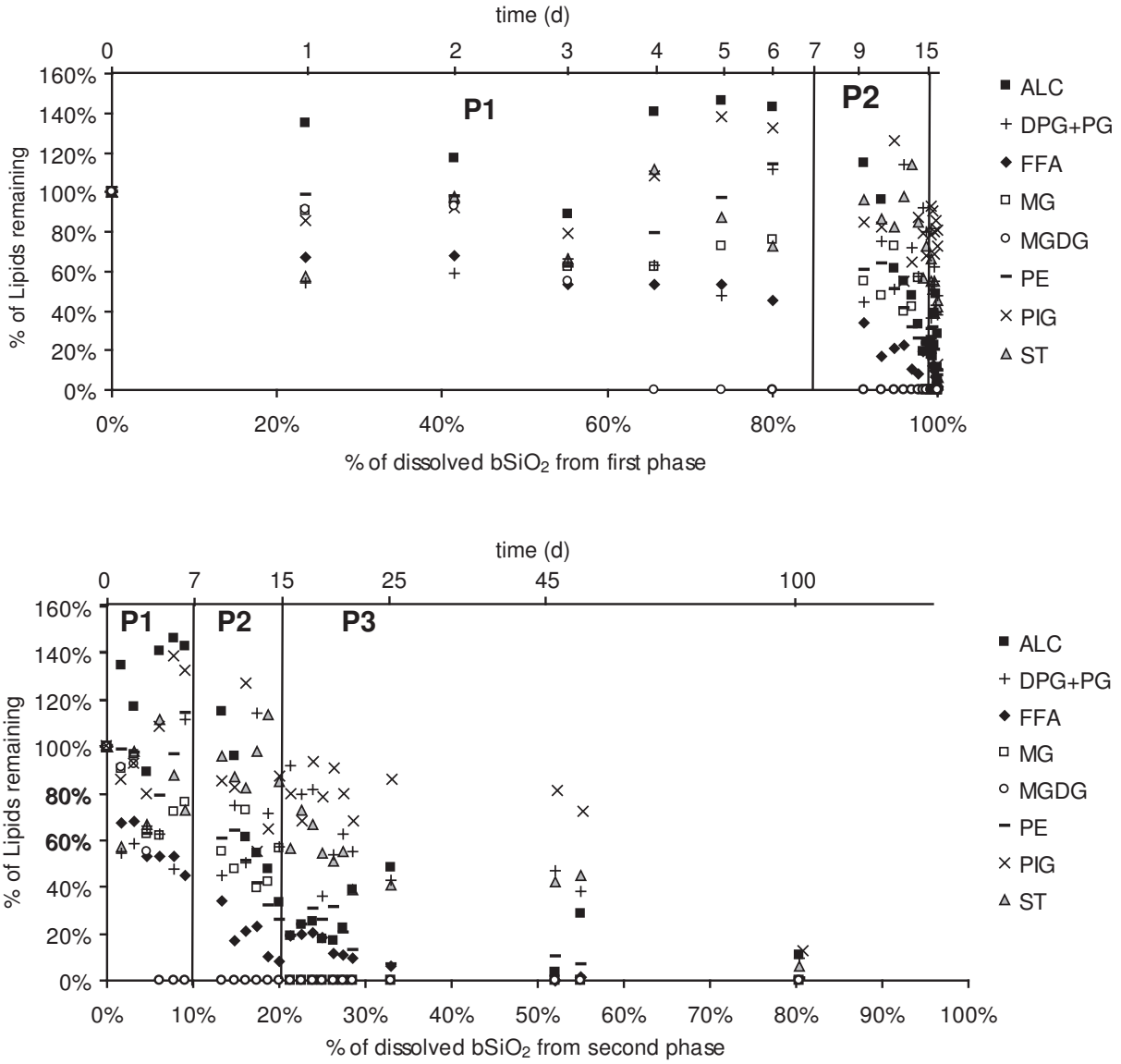

956

957

958

959

960

961

962 Fig. 8:

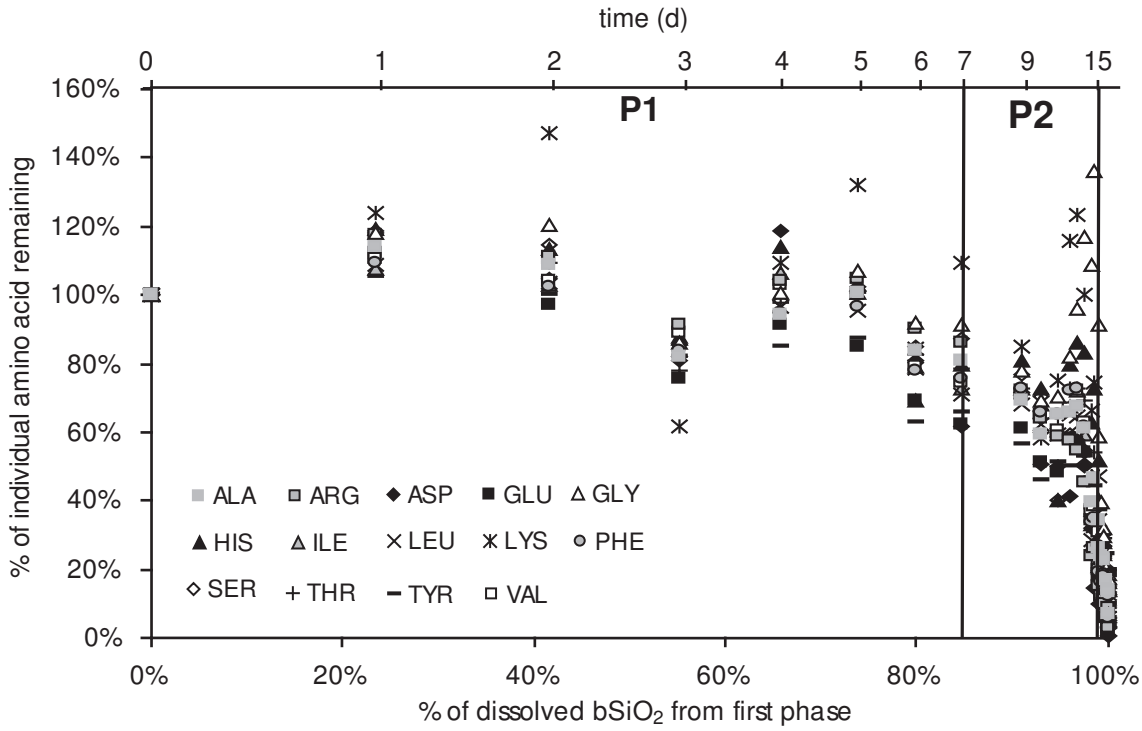

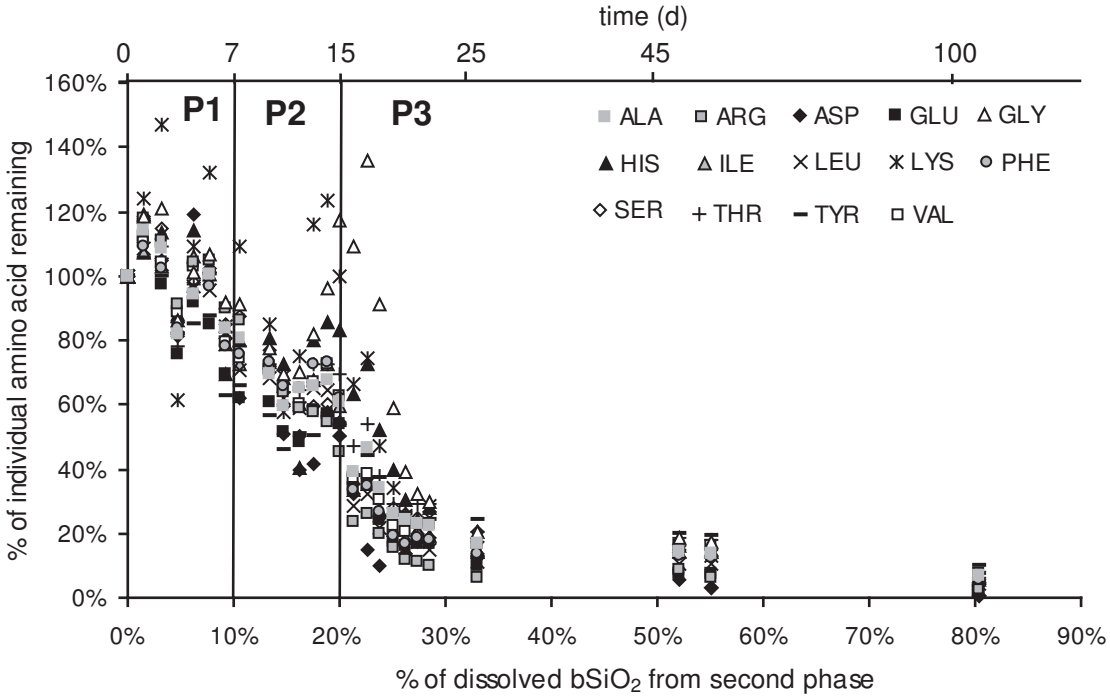

963

964